THEORETICAL INVESTIGATION OF SUPERCONDUCTIVITY IN Sr AND Na DOPED GRAPHENE SHEET

By

Mesfin Haile Mamme

A THESIS SUBMITTED TO
THE MATERIALS SCIENCE PROGRAM

PRESENTED IN PARTIAL FULFILLMENT OF THE REQUIREMENTS
FOR THE DEGREE OF MASTER OF SCIENCE

ADDIS ABABA UNIVERSITY
ADDIS ABABA, ETHIOPIA
JUNE, 2013

ADDIS ABABA UNIVERSITY
SCHOOL OF GRADUATE STUDIES
MATERIALS SCIENCE PROGRAM

We, the undersigned here by certify that we have read the thesis entitled "**THEORETICAL INVESTIGATION OF SUPERCONDUCTIVITY IN Sr and Na Doped GRAPHENE SHEET** " written by **Mesfin Haile Mamme**, and have accepted and recommended him to submit it to the School of Graduate Studies as his partial fulfillment of the requirements for the degree of **Master of Science** in Materials Science with the regulations of the University and meets the accepted standards with respect to originality.

Signed by the Examining Committee:

Dated: June, 2013

Examiner: Dr. Ahmed Mustefa, Signature: _____ Date: 04/07/2013
Examiner: Prof. Teketel Yohannes, Signature: _____ Date: 04/07/2013
Advisor: Prof. Javed Mazher, Signature: _____ Date: 04/07/2013
Chairperson: Prof. Teketel Yohannes, Signature: _____ Date: 04/07/2013

Abstract

THEORETICAL INVESTIGATION OF SUPERCONDUCTIVITY IN (Sr, Na)-GRAPHENE SHEET

Mesfin Haile Mamme

Addis Ababa University, 2013

Graphene has many remarkable properties, but superconductivity is notably absent. Recent observation of proximity effect has ignited in superconductivity of graphene sheet. In this work we explore, using density functional theory (DFT) and density functional perturbation theory (DFPT) calculation the possibility of inducing superconductivity in strontium and sodium doped graphene. We have given a clear evidence that superconductivity critical temperature T_c is easily affected by the contribution of inplane phonon vibration of intercalate and out-of-plane phonon (ZO) of the graphene sheet. Particularly Sr and Na intercalated graphene sheet leads to superconductivity, with $\lambda = 0.667$ with T_c of 7.5 K and 0.41 with T_c of 2 K for sodium and strontium intercalated graphene respectively.

Acknowledgements

I offer my deepest gratitude and special affection to my advisor Prof. Javed Mazher for his generous advise, devoted assistance, encouragement in all stages of the work, constant guidance and constructive criticism which were necessary for the progress of the research.

I would like to extend my appreciation to Prof. Teketel Yohannes for his help, support, constant guidance and constructive criticism which were necessary for the progress of the research and also in the entire study time.

I would like to thank Dr. Ahmed Mustefa for his encouragement, insightful comments, and constructive criticism.

I would like to extend my appreciation for chemistry departement specially for ENTOTO computational center for allow me to access supercomputer.

I would like to extend my appreciation for to my father capitain Haile Mamme and to all my familes for support and encouragement for the entire study.

A special thank goes to my beloved friends Gebrekirstos Gebreamlak, Fetene Fufa, Asegidaw Ergete, Gibreegziabhair Gebretsedkan, and Girma Erjabo friendly help throughout my entire study for all the good and bad times we had together.

Finally I would like to express my sincere gratitude to support and encouragement I get from Mrs. Yetnebersh Fisiha, Mr. Girmay Techane, Gasha Kiros Tewolde, Mr. Shishay Alem, Micheal Getachew, Nancy Twu and Getachew Fantahun W/o Belaynesh Bekele. They did their most keeping up the moral and material need for the success of my work.

Mesfin Haile

May, 2013

Table of Contents

List of Figures

List of Tables

Chapter 1

Introduction

Graphite has been used in pencils for several hundred years now because thin layers of it are easily exfoliated upon writing on paper. Presently, graphite finds many industrial applications, e.g. as electrodes in batteries, reinforcement material, etc. The theory predicts that single-layer graphite (graphene) is unstable under ambient conditions. Recently, high-quality graphene flakes and ribbons have been obtained by mechanical exfoliation [1] and epitaxial growth [2].

Graphene is an allotrope of carbon, whose structure is one-atom-thick planar sheets of sp^2-bonded carbon atoms that are densily packed in a honeycomb crystal lattice. Since its production in 2004, it has become the hottest research issue as it exhibits a variety of unusual physical properties such as the massless charge carrier [3], bipolar super current [4], spin injection at room temperature[5, 6] demonstrate its high potential for application in spintronic device, many physical realization of fundamental concept in Materials Science, and its outstanding electronic as well as mechanical properties.

However, in the list of graphene's many remarkable properties superconductivity is notably absent. So that, this is the first motivation to conduct this research on investigation of superconductivity in gephene sheet. If it were possible to find a way to induce superconductivity, it could improve the performance and enable more efficient integration of variety of promising device concepts including nanoscale superconducting quantum interference device, single electron superconductor quantum dot devices, nanometer scale superconducting transistor and cryogenic solid-state coolers, etc. In Addition to these, our world energy need is growing with an alarming rate, besides to this sustainable energy future through electrical energy production, storage and transmission. Most of the electrical power generated today is wasted because of resistivity losses.

Superconductivity in carbon based system has been studied substantially over the last eleven years. Diamond becomes superconducting when doping with boron [7]. Graphite and fullerenes are superconducting when intercalated with alkaline atoms [8, 9] with a record Tc = 39 K. This is also the second motivation for our research work.

Phonon mediated Superconductivity can occur in metallic system if electron-phonon interaction is large enough. The electron-phonon interaction is directly proportional to the number of carriers (the density of state at the Fermi level, N(0)) and to the coupling of the electron to the given phonon mode, namely the deformation potential, D. On the contrary the electron-phonon interaction is

proportional to the inverse of the square of the phonon frequency of the mode coupling to the electrons. So getting an optimum superconductivity under these circumstance is our last motivation to conduct this research.

To this end, we will investigate the possibility of inducing superconductivity in a graphene sheet by intercalated (doping) Sr, and Na atoms.

1.1 Graphene

Graphene is the name given to a flat monolayer of carbon atoms tightly packed into a two-dimensional (2D) honeycomb lattice, and is a basic building block for graphitic materials of all other dimensionalities as depicted in Figure 1.1. It can be wrapped up into 0D fullerenes, rolled into 1D nanotube or stacked into 3D graphite.

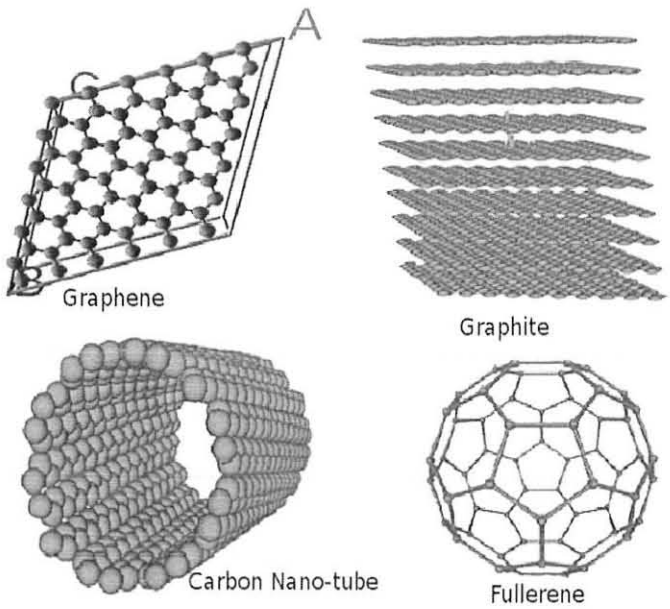

Figure 1.1: Schematic diagram of Graphene and its derivatives, Graphite, Fullernene and Carbon nanotube (CNT).

1.1.1 Structure of Graphene

Graphene consists of a single layer of carbon atoms, arranged in a honeycomb lattice. It has been studied theoretically for a long time as a building block of graphitic materials in other dimensions. The most famous allotrope of graphene is graphite, consisting of stacked graphene layers, held together only by weak Van der Waals forces. One dimensional carbon nanotubes and zero-dimensional fullerenes can be described as rolled up graphene sheets. But in contrast to these materials, isolated graphene was expected to be thermodynamically unstable and therefore not to exist in real life until its discovery in 2004 [1].

The covalent bonds between nearest-neighbor carbon atoms in graphene are formed by sp^2-hybridized orbitals. These strong bonds give graphene its extraordinary mechanical strength, making it possible to have stable free-standing graphene sheets, being only one atomic layer thick. The remaining p-electron per atom is delocalized over the whole graphene lattice, and is responsible for the electric conductivity. Figure 1.2 (a) represents the lattice structure of graphene. The graphene lattice consists of two interpenetrating sub-lattices, denoted by A and B depicted in blue (dark gray) and red (light gray). The unit cell, indicated in gray, therefore comprises two atoms, one of each sub-lattice. The nearest neighbor distance is $a_0 = 1.42$ Å. In reciprocal space, the first Brillouin zone also has a hexagonal shape as shown in Figure 1.2 (b) [10]. Valence and conduction bands touch at the K and K' points at the corners of the first Brillouin zone, with a linear dispersion for small enough energies, Figure 1.2(c). Around the K and K' points the dispersion relation of graphene can be described by the expression $E_{\pm}(\overrightarrow{q}) \approx hV_F|\overrightarrow{q}|$ with

$V_F \approx 1x10^6 ms^{-1}$. In un-doped graphene, the Fermi energy lies exactly at the Dirac point which implies that the π-band is completely filled, while the π^*- band is empty.

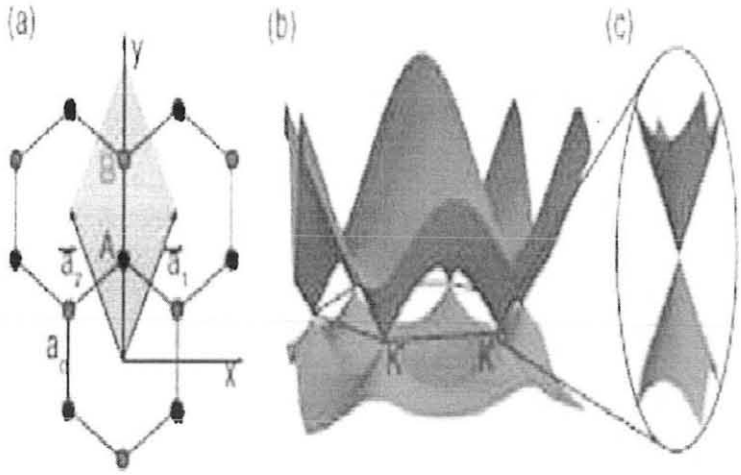

Figure 1.2: (a) Lattice structure of graphene. The atoms belonging to the two sublattices A and B are represented by circles; the lines between the circles indicate the chemical bonds. a_0 is the nearest-neighbor distance. The unit cell is depicted in light black box, together with the primitive lattice vectors a1 and a2. (b) Band structure of graphene. (c) Zoom of the dispersion relation close to the K-point for small energies [10].

This linear dispersion relation, together with the so-called pseudospin related to the two sublattices and the electron-hole symmetry, implies that the low-energy properties of graphene charge carriers can be described by the 2D massless Dirac equation $-iV_F \vec{\sigma} \bigtriangledown \psi(\vec{r}) = E\psi(\vec{r})$, where $\vec{\sigma} = (\sigma_x, \sigma_y)$ are the Pauli matrices. Although there is nothing relativistic about the electrons in graphene, the band structure resulting from the honeycomb lattice makes it possible to describe them like massless Dirac fermions, which gives rise to some of the unusual transport properties of graphene.

1.1.2 Electronic Properties of Graphene

From the point of view of its electronic properties, graphene is a two dimensional zero gap semiconductor and the low-energy charge carriers formally described by the Dirac like Hamiltonian exhibit Fermi velocity of Vf $\approx$ 1 x 10^6 m/s [11]. Neglecting many-body effects, this description is accurate theoretically and has also been proven experimentally by measuring the energy-dependent cyclotron mass in graphene (which yields its linear energy spectrum) and most clearly by the observation of a relativistic analogue of the integer quantum hall effect (QHE). The fact that charge carriers in graphene are described by the Dirac-like equation rather than the usual Schroedinger equation can be seen as a consequence of graphenes crystal structure, which consists of two equivalent carbon sub-lattices A and B as shown in the Figure 1.2(a). A quantum mechanical hopping between the sub-lattices leads to the formation of two energy bands, and their intersection near the edges of the Brillouin zone yields the conical energy spectrum near the Dirac points K and K' as shown in the Figure 1.2(b) as a result, the quasiparticles in graphene exhibit the linear dispersion relation $E = hkV_F$ as if they are massless relativistic particles, with the role of the speed of light played by the Fermi velocity $V_F \approx$ C/300. Thus owing to the linear spectrum, one can expect that these quasiparticles behave differently from those in conventional metals and semiconductors where the energy spectrum can be approximated by a paraboblic (free electron-like) dispersion relation.

1.1.3 Phonon Dispersion Relations of Graphene

Since there are two carbon atoms, A and B, in the unit cell of graphene, one must consider 6 coordinates. The secular equation to be solved is thus a dynamical matrix of rank, such that 6 phonon branches are achieved. The phonon dispersion relation of the graphene comprises three acoustic (A) branches and three optical (O) branches. The modes are associated with out-of-plane (Z), in-plane longitudinal (L), and in-plane transverse (T) atomic motions (Figure 1.3-a).

Figure 1.3-b shows the phonon dispersion branches of graphene. The three phonon dispersion branches, which originate from the Γ-point of the brillouin zone correspond to acoustic modes: an out-of plane mode (ZA), an in-plane transverse mode (TA), and in-plane longitudinal (LA), listed in order of increasing energy. The remaining three branches correspond to optical modes: one out-of plane mode (ZO), and two in-plane modes (TO) and (LO). While the TA and LA modes display the normal linear dispersion around the k-point, the ZA mode shows a q2 energy dispersion which is explained in [12] as a consequence of the D6h point-group symmetry of graphene. Another consequence of the symmetry are the linear crossings of the ZA/ZO and the LA/LO modes at the K-point. Optical mode is responsible for most optical behavior of solids. Most ionic crystals are easily excited by radiation leading to a vibrational state in which negative and positive ions oscillate out of phase with each when a solid absorbs energy, the number of phonons changes. Macroscopic properties like superconductivity, thermal energy can be described by suitable statistical models. Typical phonon energies are comparable with infrared radiation. This makes this region of electromagnetic spectrum particularly important in the context of phonons. In all interactions momentum is

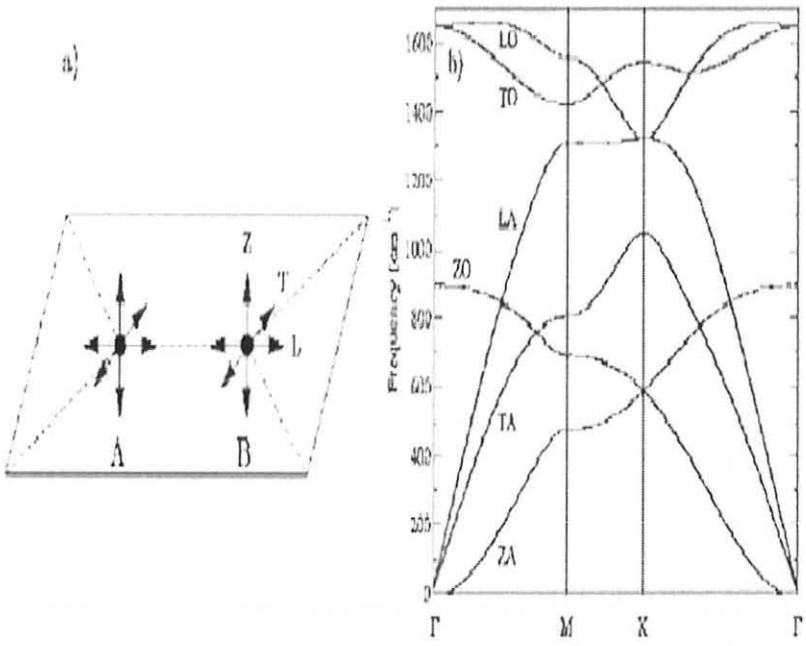

Figure 1.3: Atomic motions of carbon atoms in graphence can be along the out-of-plane (Z), in-plane transverse (T), and in-plane longitudinal (L) direction. b) The phonon dispersion branches for a graphene sheet, plotted along high symmetry directions [12].

conserved. Also from the structural point of view, graphene is not an ordinary material. The interaction between carbon atoms is made through strong sigma bonds (similar to the ones in diamond) through the overlap of the in-plane sp^2 orbitals. Because of that, graphene has a very high spring constant, K ($\sim$ 50 eV/Å^2), and its Young modulus, Y ($\sim$ 1 TPa), is one of the largest in nature. As a result, its optical phonon frequencies, ω_0 ($\sim$ 0.2 eV $\sim$ 1,600 cm^{-1}), are one of the highest among all materials. In intercalated graphene the phonon dispersion characterized by three regions: the lower energy region of adatom-related modes (up to 300 cm^{-1}) extending up to 400 cm^{-1} when mixed with carbon out-of-plane mode(Cz),an intermediate region of Cz mode (400 - 900 cm^{-1}) and higher energy region characterized by C-C starching modes, this illustrated in optical absorption

spectra of calcium intercalated graphene [13] as shown in Figure 1.4.

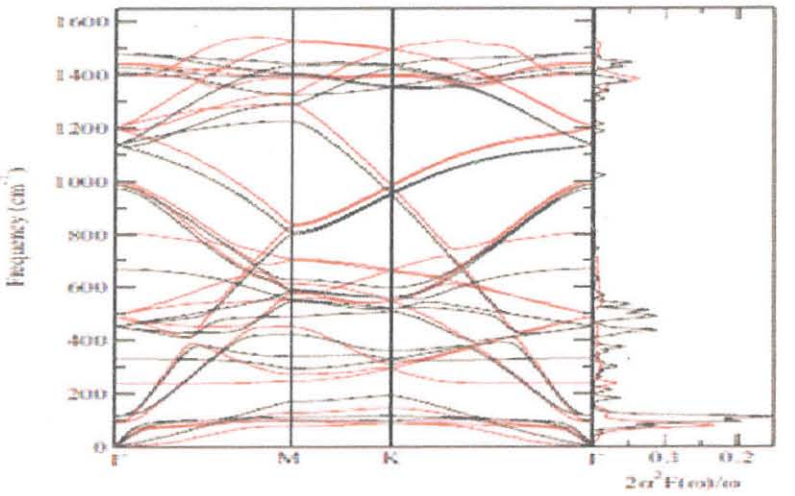

Figure 1.4: Phonon frequencies dispersion and Eliashberg function of CaC6 bulk (black) and monolayer (red) [13].

1.2 Superconductivity

Superconductor is a material that loses all resistance to the flow of electric current when it is cooled below a certain temperature, called the critical temperature or transition temperature. Above this temperature there is usually little or no indication that the material might be a superconductor. Below the critical temperature, not only does the superconductor suddenly achieve zero resistance, it gains other unusual magnetic and electrical properties. Two fundamentally important and intuitively startling properties are associated with superconductivity [14] are :-

- The transition from finite resistivity, ρ in the normal state above a superconducting transition temperature T_c to $\rho = 0$, i.e. perfect DC conductivity, $\sigma = \infty$, below T_c.

• The simultaneous change of magnetic susceptibility χ from a small positive paramagnetic value above T_c to $\chi = -1$, i.e. perfect diamagnetism below T_c.

These aspects are qualitatively illustrated in Figure 1.5:

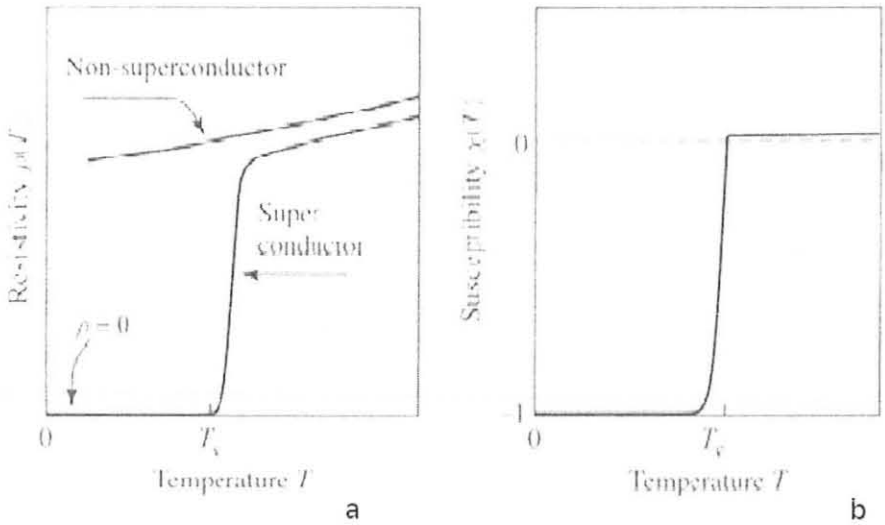

Figure 1.5: Sketches of the two basic characteristics of a superconductor [14, 15] (a) shows the drop to zero resistivity at a temperature Tc, compared to a non superconducting behavior. (b) shows the corresponding drop in susceptibility to the ideal diamagnetic value of χ = -1 below Tc. The onset of the diamagnetic response corresponds quite closely to the point where R 0 on the temperature axis. The figure also indicates that χ is positive but quite small above Tc.

1.3 Superconductivity Theory

BCS Theory

The understanding of superconductivity was advanced in 1957 by three American physicists, John Bardeen, Leon Cooper, and John Schrieffer, through their theories of superconductivity, know as the BCS Theory [14, 15]. The BCS theory explains superconductivity at temperatures close to absolute zero. Cooper realized that atomic lattice vibrations were directly responsible for unifying the

entire current. They forced the electrons to pair up into teams that could pass all of the obstacles which caused resistance in the conductor.

These teams of electrons are known as Cooper pairs [14, 15]. Cooper and his colleagues knew that electrons which normally repel one another must feel an overwhelming attraction in superconductors. The answer to this problem was found to be in phonons, packets of sound waves present in the lattice as it vibrates. Although this lattice vibration cannot be heard, its role as a moderator is indispensable.

According to the theory, as one negatively charged electron passes by positively charged ions in the lattice of the superconductor, the lattice distorts. This in turn causes phonons to be emitted which form a trough of positive charges around the electron [15]. Figure 1.6 illustrates a wave of lattice distortion due to attraction to a moving electron.

Before the electron passes by and before the lattice springs back to its normal position, a second electron is drawn into the trough. It is through this process that two electrons, which should repel one another, link up. The forces exerted by the phonons overcome the electrons' natural repulsion. The electron pairs are coherent with one another as they pass through the conductor in unison. The electrons are screened by the phonons and are separated by some distance. When one of the electrons that make up a Cooper pair and passes close to an ion in the crystal lattice, the attraction between the negative electron and the positive

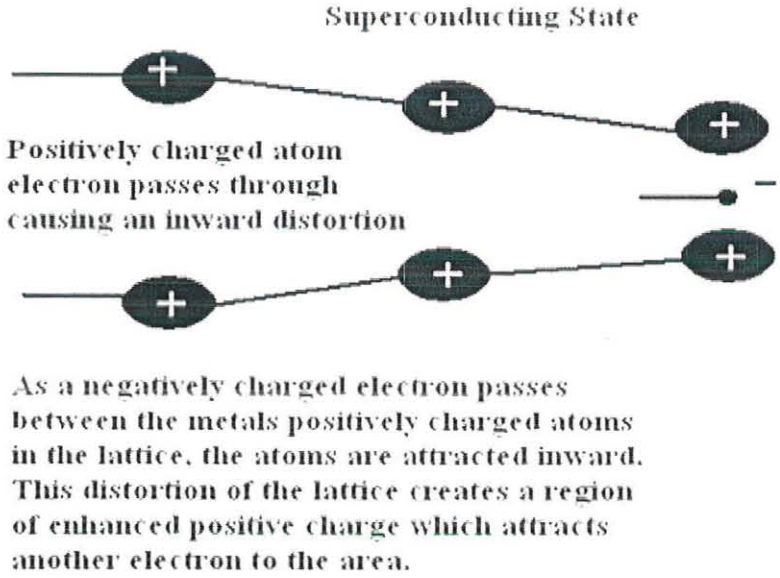

Figure 1.6: BCS theory [15, 16].

ion cause a vibration to pass from ion to ion until the other electron of the pair absorbs the vibration [15]. The net effect is that the electron has emitted a phonon and the other electron has absorbed the phonon. It is this exchange that keeps the Cooper pairs together. It is important to understand, however, that the pairs are constantly breaking and reforming. Because electrons are indistinguishable particles, it is easier to think of them as permanently paired. Figure 1.7 illustrates how two electrons, called Cooper pairs, become locked together.

The BCS theory successfully shows that electrons can be attracted to one another through interactions with the crystalline lattice. This occurs despite the fact that electrons have the same charge. When the atoms of the lattice oscillate as positive and negative regions, the electron pair is alternatively pulled together and pushed apart without a collision. The electron pairing is favorable because it has the effect of putting the material into a lower energy state. When electrons are linked

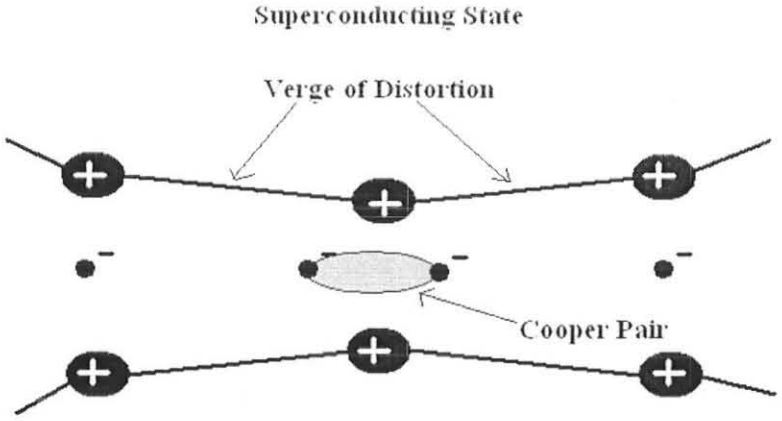

Figure 1.7: BCS theory (Cooper pairs) [15].

together in pairs, they move through the superconductor in an orderly fashion.

1.4 Electron-phonon interaction

We saw that in the BCS theory phonons play an important role to describe the superconducting state. In the Eliashberg theory the electron phonon coupling constant λ_{eph} allows one to write the effective mass m = m(1+λ_{e-ph}) [16]. λ_{eph} is due to phonon contributions, each weighted with the spectral function (Eliashbergs function) $\alpha^2F(\omega)$, as one can see in Equation (1.4.1). $F(\omega)$ is the phonon density of states and α^2 is the matrix describing the electron-phonon interaction.

$$\lambda_{e-ph} = 2\int \frac{d\omega}{\omega}\alpha^2F(\omega) \tag{1.4.1}$$

Let us consider, for strong electron-phonon interaction, only the electrons near the Fermi surface and a phonon with wave vector q and frequency ν. The interaction can be written through an average, on the Fermi surface, of the interactions of each electron with the phonons. The matrix elements of the electron-phonon

interaction are included in

$$\gamma^{q\nu} = 2\pi\omega_{q\nu} \sum_{kjj'} |g^{q\nu}_{k-qjikj}|^2 \, \delta(\epsilon_{kj} - \epsilon_F)\delta(\epsilon_{kj-qj} - \epsilon_F) \tag{1.4.2}$$

and can be written as $g^{q\nu}_{k-qjikj}$. The spectral function is a density of phonon states weighted with the coupling of each phonon with the electrons on the Fermi surface and can be written as the sum of each term $\gamma^{q\nu}$ weighted with the phonon frequency, commonly, known as eliashberg function,

$$\alpha^2 F(\omega) = \frac{1}{2\pi N(\varepsilon_F)} \sum_{q\nu} \frac{\gamma_{q\nu}}{\omega_{q\nu}} \delta(\omega - \omega_{q\nu}) \tag{1.4.3}$$

The strong coupling with a generic phonon of frequency ω_{ph} gives rise to a peak in the spectral function at ω_{ph}. Then, we can write the total electron-phonon coupling constant λ_{e-ph} by considering all the contribution $\lambda_{q\nu}$ of each phonon:

$$\lambda_{q\nu} = \frac{\gamma^{q\nu}}{\pi N(\epsilon_F)\omega^2_{q\nu}} \tag{1.4.4}$$

$$\lambda_{e-ph} = \sum_{q\nu} \lambda_{q\nu} \tag{1.4.5}$$

Each coupling q gives a contribution to define the Tc [16], as shown by the McMillan- Dynes formula in Equation (1.4.7) where the free parameter μ^* takes into account the screening of the Coulomb interaction. The frequency ω_{ln} is a logarithmic average of the phonon frequencies defined in Equation (1.4.6). These calculations allow one to obtain an expected Tc [16] to be compared with experimental results.

$$\omega_{ln} = exp\left(\frac{\sum_{q\nu} \lambda_{q\nu} ln\omega_{q\nu}}{\sum_{q\nu} \lambda_{q\nu}}\right) \tag{1.4.6}$$

$$T_c = \frac{\omega_{ln}}{1.2} exp\left(-\frac{(1 + \lambda_{e-ph})1.04}{\lambda_{e-ph} - \mu^*(1 + 0.62\lambda_{e-ph})}\right) \tag{1.4.7}$$

1.5 Contemporary trends in Graphite and Graphene superconductivity

Many research groups are studying Superconductivity in different materials, including graphite. It was also found that alkaline earth GICs (Graphite Intercalated Compounds) exhibit superconductivity [17, 18] with a transition temperature of 6.5 K (YbC_6) and 11.5 K (CaC_6). Careful analysis [19 - 22] of the electron-phonon coupling in CaC_6 reveals that this superconductor is of the conventional BCS type, and that the presence of both Ca-derived and C-derived bands is necessary to explain the relatively high superconducting transition temperature in this compound. It should be pointed out, however, that some controversy still exists regarding the mechanism for superconductivity in CaC_6 GIC. Whereas a large Ca isotope effect was measured in CaC_6 GIC [23, 24] indicating a dominant role played by phonons due to Ca atomic vibrations, angle-resolved photoemission spectroscopy (ARPES) measurements on CaC_6 GIC [25], on the other hand, indicate that graphitic high frequency phonon modes are most strongly coupled to electrons. The recent discovery of stable graphene sheets [26] raises the question of whether two-dimensional superconductivity is possible in intercalated graphene layers. The possibility of intercalating a system consisting of a few graphene layers with intercalants, such as $FeCl_3$, Br, and Li has been recently demonstrated [27 - 29]. Doping of graphene, via the addition of potassium adatoms, has also been demonstrated [30]. It is clear that a system consisting of many graphene layers, if intercalated, should exhibit properties similar to those of GICs. It is natural to ask whether a system consisting of a few graphene layers, intercalated with alkali, or alkaline earth metal atoms, will

exhibit superconductivity. This problem was discussed recently by Mazin and Balatsky [31], who considered a graphene bilayer intercalated with Ca. They argued, on the basis of similarities with the electronic energy bands of the CaC_6 GIC, that a graphene bilayer intercalated with Ca is probably a superconductor.

Other Groups, in California university examine the problem of superconductivity in intercalated graphene layers [32]. In particular, they calculated the bands in a graphene bilayer intercalated with the alkaline earth atoms Ca, Sr, and Ba [32]. In all three cases, they found a band, derived from the alkaline earth atoms, crosses the Fermi energy, along with carbon-derived π-bands, then calculate the electron-phonon coupling strength λ in these systems. The values they obtained are reasonably large; in the case of Ca-intercalated bilayer, they found $\lambda = 0.60$, a value to be compared with 0.83 calculated in CaC6 GIC [32]. In addition to these, they studied the case of a graphene trilayer intercalated with Ca and they found a value of $\lambda = 0.80$ for the electron-phonon coupling strength λ. These calculations indicates that superconductivity is indeed possible in intercalated graphene layers.

1.6 Applications of Superconductors

Superconductivity is widely regarded as one of the great scientific discoveries of the 20th Century. This miraculous property causes certain materials, at low temperatures, to lose all resistance to the flow of electricity. This state of losslessness enables a range of innovative technology applications. At the dawn of the 21st century, superconductivity forms the basis for new commercial products that are transforming our economy and daily life.

Current Commercial Applications are:

- Magnetic Resonance Imaging (MRI)
- Nuclear Magnetic Resonance (NMR)
- High-energy physics accelerators
- Plasma fusion reactors
- Industrial magnetic separation of kaolin clay

The major commercial applications of superconductivity in the medical diagnostic, science and industrial processing fields listed above are all involve low temprature superconductor (LTS) materials and relatively high field magnets. Indeed, without superconducting technology most of these applications would not be viable. Several smaller applications utilizing LTS materials have also been commercialized, example magnets and Magneto-Encephalograhy (MEG). The latter is based on Superconducting Quantum Interference Device (SQUID) technology which detects and measures the weak magnetic fields generated by the brain. The only substantive commercial products incorporating HTS materials are electronic filters used in wireless base stations. About 10,000 units have been installed in wireless networks worldwide to date.

Some of the Emerging Applications of superconductors [33] are :

Superconductor-based products are extremely environmentally friendly compared to their conventional counterparts. They generate no greenhouse gases and are cooled by non-flammable liquid nitrogen (nitrogen comprises 80% of our atmosphere) as opposed to conventional oil coolants that are both flammable and toxic. They are at least 50% smaller and lighter than equivalent conventional

units which translates into economic incentives. These benefits have given rise to the ongoing development of many new applications in the following sectors:

- Electric Power: Superconductors enable a variety of applications to aid our aging and heavily burdened electric power infrastructure for example, in generators, transformers, underground cables, synchronous condensers and fault current limiters. The high power density and electrical efficiency of superconductor wire results in highly compact, powerful devices and systems that are more reliable, efficient, and environmentally benign.
- Transportation: The rapid and efficient movement of people and goods, by land and by sea, poses important logistical, environmental, land use and other challenges. Superconductors are enabling a new generation of transport technologies including ship propulsion systems, magnetically levitated trains, and railway traction transformers.
- Medicine: Advances in HTS promise more compact and less costly Magnetic Resonance Imaging (MRI) systems with superior imaging capabilities. In addition, Magneto-Encephalography (MEG), Magnetic Source Imaging (MSI) and Magneto-Cardiology (MCG) enable non-invasive diagnosis of brain and heart functionality.
- Industry: Large motors rated at 1000 HP and above consume 25% of all electricity generated in the world. They offer a prime target for the use of HTS in substantially reducing electrical losses. Powerful magnets for water remediation, materials purification, and industrial processing are also in the demonstration stages.

• Communications: Over the past decade, HTS filters have come into wide spread use in cellular communications systems. They enhance signal-to-noise ratios, enabling reliable service with fewer, more widely-spaced cell towers. As the world moves from analog to all digital communications, LTS chips offer dramatic performance improvements in many commercial and military applications.

Chapter 2

OBJECTIVES

General Objective

To investigate superconductivity in graphene sheet by intercalating Na and Sr atoms.

Specific Objectives

- Prepare Model of pristine, Na and Sr intercalated graphene sheet.

- Optimize the structure of pristine and intercalated graphene sheet.

- Calculate Electron density of state, phonon dispersion and phonon DOS of pristine and intercalated graphene.

- Calculate electron-phonon coupling strength and superconductivity critical temperature Tc of Na and Sr doped graphene sheet.

Chapter 3

COMPUTATIONAL REVIEW

3.1 Introduction

If the aircraft technology would have advance at the same speed that of computer technology, it would be possible to get Boeing 747 that would be large enough to carry 12,000 people to the moon in about few hours for the round trip costs of that is cheaper than any transportation. Thus, computer technology, particularly in the area of increasing speed of calculation and more efficient memory storage device, has improved at a whirlwind pace over the past 30 years. Many of the improvements in computer hardwares and the algorithms (softwares) that control the computers have presented a new tool for scientific investigations.

Computational materials science and engineering (CMSE) is a relatively young field. The first known case study of materials that used digital computers was made shortly after the Second World War. The legendary mathematician John von Neumann at the wartime Los Alamos National Laboratory is credited as being the first to seriously consider numerical methods and encourage using computing machines. Not surprisingly, early material simulations stemmed directly from the war efforts. One of the focuses of research at the time was

on how irradiation of high-energy particles would change a materials structure and properties, an obviously urgent topic at the time. Nevertheless, the activities in this relatively obscure and small area remained dormant until the sixties when faster and more powerful digital computers became available. Now computational materials science is an active and fast-growing field. It covers many topics in nearly all branches of materials science and engineering. As its impact has grown, it has gained a reputation as being the third approach for scientific research and engineering, parallel to experiment and theory.

Compared to humans, computers are more efficient and less error-prone in handling repetitive or numerical tasks. For this reason, computers are used extensively in materials research (and other fields as well) to do such tedious work as data acquisition and data analysis. Computational materials science and engineering is, however, more striving in its objectives and much broader in its scope. Its aim is to understand and predict the physical-properties relationships of materials in various length scales, from not only the continuum (millimeters and up) level, but also from the mesoscopic (microns) and atomic (nanometers and Angstroms) levels. For instance, to materials scientists and engineers, the stress-strain relation is no longer the end in the pursuit of the mechanical properties of the materials. Now, using their understanding of stress-strain relations and microstructure, researchers seek to answer more complex questions such as how microstructures become what they are under different conditions, what dislocation cores look like, and how detailed interatomic interactions influence the microstructure and defect structures etc...

Furthermore, the unique capability of computer simulations and modeling allows us to see materials not only better on smaller scales but also more quantitatively. With properly constructed models (Hamiltonian or interatomic interaction), one can simulate, or mimic, the entire physical process of the model materials, including microstructure evolution, deformation process, defect structure, or phase transitions. From the known constitutive relations, one can model a large number of material behaviors, ranging from mechanical deformation, magnetism, superconductivity and chemical reaction, to piezoelectrics. Remarkable progress has been made in computational materials science and engineering over the last two decades. Driven by our desire to know more and by the ever-increasing power in digital computer, new frontiers in materials modeling are constantly being explored using numerical methods. Among these new areas are simulations of nanoscale materials, glasses, soft and polymeric matters, granular matter, strongly disordered systems, non-equilibrium systems and driven phenomena. These topics pose new challenges that demand development of new simulation methods in mesoscopic scales, efficient platforms in hardware, and faster and efficient software to break the barrier of size and time limitations in atomistic and quantum simulations. Breakthroughs in these areas could finally bring the materials simulation and modeling to a new level where computational experiments could be conducted hand in hand with real experiments. The only difference one will notice is that the materials used in the experiment are digital materials, which are much cheaper and easier to make and pose no danger to our health or environment.

My research is in the area of Nanotechnology, so that am trying to shift the review direction to the atomistic quantum mechanics calculations of computational materials science. Depending on Atomistic simulation we can explore different problems in materials science and find noble intrinsic properties by changing size, dopant, shape, and structure of materials. In this case computational materials science contributes a lot for materials science especially for the innovation of noble materials.

The important contribution to the field is that, it can predict materials properties even before actual material process. Therefore, these saves time, laboratory materials cost, human resource and instruments for synthesizing materials. In addition to these, this technique is environmentally friendly. In some case there are some samples which are not easily prepared in laboratory, but it is possible in computational materials science even if it is more complicated, we can study and determine their properties. There are some difficulties that are faced in computational materials science, because of the reason, it requires supercomputer that is costly, high speed processor, finding exact solution for many body system without approximation is impossible, so it uses some approximation to show the trained, in the next section we will see different approximations. Within those approximations we can efficiently find the trained of new materials. Many of the problems of Materials Science and Engineering are solved by computational materials science. Some of these are:

- Geometrical optimization
- Phonon calculation

- Electronic structure
- Band structure and
- Density of state calculation.

The central idea of Quantum Mechanics in Materials science is to find the solution of SchrÖdinger Equation (3.1.1) of the many body system, which is exact or approximated.

$$[-\frac{\hbar^2}{2m} \bigtriangledown^2 + V(r)]\psi(r) = E\psi(r) \tag{3.1.1}$$

Where terms in the bracket is correspond to kinetic energy and potential energy respectively. By the way, there is no mathematical proof for SchrÖdinger equation, but its success is due to high accuracy solving the experimental work. In the coming subsection we will trying to discuss some of the computational technique and approximation.

3.2 Theories and Approximation in Many Body Calculations

In many body systems the properties of the materials explored using computational method are from the motions of electron to nuclei. But, nuclei are much massive than electron, so we can consider motions of electron separate from that of nuclei called Born and Oppenheimer Aproximation.

3.2.1 Born-Oppenheimer Approximation

The adiabatic approximation of Born and Oppenheimer allows one to treat the electrons and nuclei of a real system separately as a consequence of the large mass difference between them [34]. Being much lighter than the ions, the electrons

move in a solid much faster than the nuclei, which make it possible to consider the electronic configuration as completely relaxed in its ground state at each position of the ions during their motion. Thus the nuclei can be treated adiabatically, leading to a separation of the electronic and nuclear degrees of freedom in the many-body wave function. The only exception to this are the lightest elements (especially hydrogen), where the ions require quantum mechanical treatments. Although the Born Oppenheimer approximation provides a major simplification to the complicated many-body problem by transforming it into the solution of the electronic dynamics in some frozen configuration of nuclei, further approximations are required to perform efficient and accurate total energy calculations. Essentially these lead to find some other many body approximation.

3.2.2 Hartree Energy

The Born-Oppenheimer approximation begins to outline a many-body Hamiltonian in a useful manner by reducing out various terms. But the many-body problem is a complex one and the Hamiltonian derived in the Born-Oppenheimer is still not suitable for calculations. There are further approximations that must be made to achieve better accuracy and minimize calculation time. That is what is involved in the derivation of the Hatree Energy equations [35]. As was mentioned previously the SchrÖdinger wave equation will be used to solve for the energy of the many-body solid. First, take the Hamiltonian that is defined in the Born-Oppenheimer approximation and put it into the SchrÖdinger equation with a new wave function. Then to define a wave function as a new combination of products of the wave functions that correspond to individual electrons. It can be written

as,

$$\psi = \phi_1(\chi_1)\phi_2(\chi_2)\phi_3(\chi_3).....\phi_n(\chi_n). \tag{3.2.1}$$

However this wavefunction cannot be put straight into the SchrÖdinger wave equation without some analysis and manipulation. The first step is to use the variational principle to analyze and set the energy of a system involving these wave functions. Our overall goal is to find the ground state and the variational principle places a limit on the minimum energy of the system. It outlines the equation below, where it is defined as,

$$E = \frac{\langle\psi|H|\psi\rangle}{\langle\psi|\psi\rangle} \tag{3.2.2}$$

Where E $\geq E_0$ and E_0 is the ground state energy of the system. From this it is possible to get an energy minimum. However that minimum is not necessarily the ground state energy. This method using this variational principle one can derive the Hartree energy equation using these equations and the variational principle it is possible to derive the Hartree energy equations, however it is more useful to include the Pauli-Exclusion principle.

3.2.3 Hartree Fock Theory

The Hartree energy equations can be useful under some specific circumstances, but they still lack some important characteristics. Primarily, the lack of spin is troubling. It can be included in a post analysis. However, an ad-hoc solution and does not contain useful information. Spin characteristics into the wave function from

the beginning. It can be done by using what is called the Slater determinant[35].

$$\psi(\chi_1, \chi_2, \chi_3, \ldots \chi_n) = \frac{1}{\sqrt{N!}} \begin{vmatrix} \phi_1(\chi_1) & \phi_2(\chi_1) & \ldots & \phi_n(\chi_1) \\ \phi_1(\chi_2) & \phi_2(\chi_2) & \ldots & \phi_n(\chi_2) \\ \ldots & \ldots & \ldots & \ldots \\ \phi_1(\chi_n) & \phi_2(\chi_n) & \ldots & \phi_n(\chi_n) \end{vmatrix} \tag{3.2.3}$$

A Slater determinant, as in above is n by n matrix that includes the Pauli exclusion principle, which is essential if each state has to be unique. If ji = ij then two columns of the determinant would be 0. This is desirable to be sure that a non-physical situation such as the equality of two different states cannot happen. It can be written in a more straightforward fashion with a permutation operator such that,

$$\psi(\chi_1 \ldots \chi_n) = \frac{1}{\sqrt{n!}} \Sigma_p (-)^p P(\Phi_1(\chi_1)\Phi_2(\chi_2)\ldots\Phi_n(\chi_n)) \tag{3.2.4}$$

This permutation operator works by switching either the coordinates or the subscripts of the wave functions. Keep in mind that these individual wave functions are orthogonal in a manner such that,

$$\langle \psi_i(r_k) | \psi_j(r_k) \rangle = \delta_i j \tag{3.2.5}$$

is true. Using this information and methodology it is possible to derive the Hartre-Fock Equations, which minimized in to,

$$(\frac{-\hbar^2}{2m} + V_H(r) + V(r) + V_x(r))\phi_i(r) = E_i \phi_i(r) \tag{3.2.6}$$

where the $V_H(r')$ term is the Coulomb repulsion term which can be written as,

$$V_H(r') = e^2 \int \frac{n(r')}{r - r'} d^3 r' \tag{3.2.7}$$

These equations are useful but still lack an approximation for the exchange correlation potential, which is addressed in density functional theory (DFT) in the next section.

3.3 Density Functional Theory (DFT)

Now that the fundamentals of the Hartree-Fock and the Hartree energy equations have been reviewed, there is a system of equations that covers the many-body problem between the electrons and the ions in a solid. The equations that have been derived are correct, but have a large number of variables and are therefore not useful. For example the wavefunction of each electron in a solid would need to be solved and a solid of any significant volume would have a number of electrons on the order of Avogadros number. This is an impractical number of equations to solve; so in order to find a useable solution one needs to find a way to condense these equations. Hohenberg, Kohn and Sham together developed a method to deal with the many-body problem. This approach involves a method that relies on electron functionals [34, 36]. The Hohenberg-Kohn theorem dictates that a potential can be determined uniquely from the ground state electron density [34, 36]. It also goes on to say that the reverse is true. From a known potential one can determine the electron density. One knows this because a definite electron potential fixes the Hamiltonian, which is known from the existence theorem. The existence theorem states that a density functional uniquely determines the Hamiltonian. The software uses density functional theory as the basis of the solutions. So a functional needs to be defined. A functional takes a function and defines a single number from the function, such as,

$$F[f] = \int_{-1}^{1} f(x)dx \tag{3.3.1}$$

So the Hohenberg and Kohns theorem is such that a ground state energy can be expressed as E[n(r)] where n(r) is the electron density and hence the reason for the

name density functional theory [37]. That means, one needs to come up with an expression for n(r). This is where the Thomas-Fermi contribution to the theory needs to be outlined, which will illuminate further practical steps. Thomas and Fermi posited that the electron density is uniquely determined by the potential. To start, one need to know the density of states as in,

$$N = V \sum_{\sigma} dkn(k) = \frac{1}{2\pi^3} k_f V \tag{3.3.2}$$

This is a well-known equation. It outlines the the amount of energy states that electrons can occupy in a given volume. When one know the density of states one can estimate the kinetic energy of particles in the system. From the kinetic energy it is possible to estimate the potential. However this estimation is not complete, for example there is something called exchange correlation energy that is not included, and that leads to large systematic errors in the final answers. The exchange correlation energy is actually two terms that have been combined into one energy. Both energies are unknown in the current formalism and must be approximated, so to simplify matters they have been combined. An exchange energy refers to the exchange interaction theory. In that theory, particles with overlapping wavefunctions of identical particles have different energies than expected. The correlation energy is often referred to as the Coulomb correlation and has to do with the coulombic repulsion spatial characteristics of electrons. One of the primary goals of density functional theory is to come up with a good approximation of the exchange-correlation energy, which will be discussed more in the Local Density Approximation section.

The Kohn-Sham (KS) energy functional is written as:

$$E[n] = T[n] + \int drn(r)Vext(r) + 1/2 \int drdr' \frac{n(r)n(r')}{|r - r'|} + E_{xc}[n] \qquad (3.3.3)$$

where terms correspond to the kinetic energy, the energy of the external potential, the Coulomb interaction between electrons, and the exchange-correlation energy, respectively. If we consider the kinetic energy to be computed in the absence of electron-electron interactions, and apply the variational principle to Equation (3.3.3), we are led the Kohn-Sham (KS) equations:

$$[-\frac{\nabla^2}{2} + \int dr' \frac{n(r')}{|r - r'|} + V_{ext}(r) + V_{xc}(r)]\psi(r) = \epsilon_i \psi_i(r) \qquad (3.3.4)$$

where $n(r)$ is the total electron density, V_{xc} is the exchange-correlation functional, $\psi_i(r)$ are the single electron KS wavefunctions, ϵ_i are the eigen values, and V_{xc} is any external potential including the pseudopotential that defines the atomic core and the applied bias potential that drives current flow. We have also introduced the exchange-correlation potential:

$$V_{xc}[n] = \frac{\delta E_{xc}[n]}{\delta n(r)} \qquad (3.3.5)$$

and can identify the term in brackets of Eq.(3.3.4) as the KS Hamiltonian.

The strength of DFT lies in the fact that the interacting many-electron problem has been reduced to a set of KS equations involving non-interacting electrons moving in the effective potential of the other electrons. Furthermore this mapping is exact provided that the exact exchange-correlation functional is known. In principle, the exact exchange-correlation functional is far too complicated to ever express in a closed form, and therefore approximations must be used. The

simplest approximation to the exchange-correlation functional is the local density approximation (LDA) [38, 39], in which one approximates the non-classical corrections to the energy with the energy density of a homogeneous electron gas.

3.3.1 Kohn Sham Equations

The Kohn-Sham equations are often broken down into three equations that give essentially the same information as the Hartree and Hartree-Fock equations. However this new equation is a single equation *versus* the many-body equations in the previous versions. Keep in mind that these two methods are not equivalent. The Kohn-Sham enable a mapping of the original Hartree Fock equations that can yield a similar answer. Which is the ground state electron density of the system. Density functional theory is only capable of determining the ground state density of the system. If an excited state is desired it is possible to figure that out from the ground state.

Next the Kohn-Sham equations need to be derived. Fortunately, however, the procedure to derive them is very similar to the process shown in the derivation of the Hartree and Hartree-Fock methods. It involves the variational principle and minimizing the expectation value of the Hamiltonian. For the sake of the simplicity only the solution and salient points will be given [40]. The Kohn-Sham equations end up giving a set of equations similar to the Euler-Lagrange equations seen in classical mechanics. However the variable, that would normally be used in the Euler-Lagrange is replaced by a wavefunction. It can be seen through the variational method that these equations based on the new functional definition of

the energy start as,

$$F[n] = F_{KE}[n] + E_{xc}[n] + \frac{e^2}{2}\int \frac{n(r)n(r')d\tau d\tau'}{|r-r'|} \tag{3.3.6}$$

Knowing this one can then obtain the Euler-Lagrange equations for this system as

$$\frac{\delta F_{KE}[n]}{\delta n(r)} + V_{eff}(r) = \mu \tag{3.3.7}$$

Which when one substitutes in,

$$n(r) = \sum_{j=1}^{N} |\phi_j(r)|^2 \tag{3.3.8}$$

as the electron density, we can then obtain one form of the Kohn-Sham Equation as,

$$(-\frac{1}{2}\bigtriangledown^2 + V_{eff}(r) - \epsilon_j)\phi_j(r) = 0 \tag{3.3.9}$$

3.3.2 Local Density Aproximation (LDA)

Now it is a crucial to mension about exchange correlation approximation. There are many exchange correlationapproximation, one of the popular approximation is LDA. This approximation can help to actually calculate the electron density as if it were a uniform electron gas with the density of states as mentioned above. Over a small enough regions one can always make this approximation. From a summation over all the regions it is possible to get an approximate expression for the entire solid. So first one wants to write down an effective potential such that,

$$V_{eff}(r) = V(r) + \int \frac{n(r')}{|r-r'|}dr' + V_{xc}(r) \tag{3.3.10}$$

This is the same effective potential as before. The next step is to write down a new exchange correlation energy for this approximation which can be written as

$$E_{xc}^{LDA} = \int n\epsilon_{xc}^{u}[n(r)]dr \tag{3.3.11}$$

Keep in mind that this exchange energy is representative of the energy for each particle. This new energy can be rewritten as, Vxc(r) as

$$V_{xc}(r) = \frac{\delta E_{xc}[n]}{\delta n(r)} \tag{3.3.12}$$

In computational process we can follow an iteration calculation; A flowchart illustrating a self-consistent DFT calculation is shown in Figure below, the calculation begins with a trial electron density.

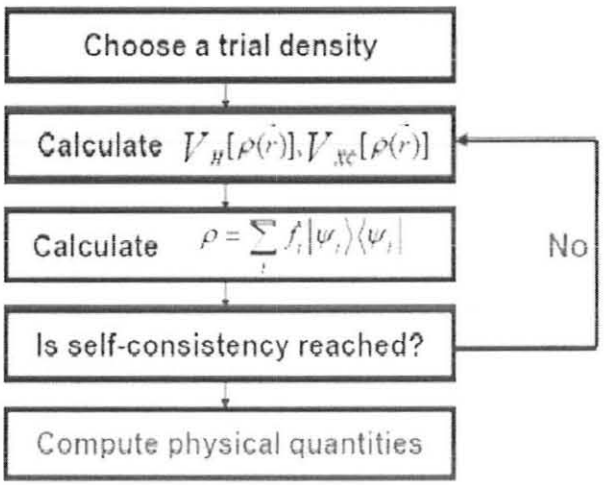

Figure 3.1: SCF calculation

3.3.3 Generalised Gradient Approximation (GGA)

In the generalised gradient approximation (GGA) a functional form is adopted which ensures the normalisation condition and that the exchange hole is negative definite. This leads to an energy functional that depends on both the density and its gradient but retains the analytic properties of the exchange correlation hole inherent in the LDA.

The typical form for a GGA functional is;

$$E_{xc}^{GGA} = \int n(r)\epsilon_{xc}[n(r), \bigtriangledown n]dr \tag{3.3.13}$$

GGA improves significantly on the LDAs description of the binding energy and energy band structure of the system.

3.4 Density Functional Perturbation Theory (DFPT)

Many physical properties depend upon a system response to some form of perturbation. Examples include polarisabilities, phonons, Raman intensities and infrared absorption cross-sections to name but a few. Density functional perturbation theory (DFPT) is a particularly powerful and flexible theoretical technique that allows calculation of such properties within the density functional frame work, there by facilitating an understanding of the microscopic quantum mechanical mechanisms behind such processes, as well as providing a rigorous testing ground for theoretical developments. System responses to external perturbations may be calculated using DFT with the addition of some perturbing potential because of the fact that to realized the electron-phonon coupling; however, as such methods involve obtaining the system response through a series of single-point energy calculations carried out at varying strengths of the external perturbation, it can be said that they are some what crude and aesthetically unappealing. More fundamentally, such techniques are sometimes restricted in application: for example, they cannot readily be used to calculate the response of crystalline systems to electric field perturbations, and cannot, without large computational effort, calculate phonon responses at arbitrary wave vector; crystalline points which will be expounded upon in this thesis. We now consider the application of perturbation

theory to DFT for calculation of the exact phonon and electron-phonon coupling responses within crystalline materials.

The two main formalisms of DFPT are due to Baroni [41] and Gonze [42]; although the two may be shown to be equivalent, there are differences in the implementation that may result in one method being preferable to another. The Gonze formalism is centred upon obtaining a series of equations that may be solved self-consistently using Green's function methods; the Baroni formalism is based rather upon a perturbative expansion of the Kohn-Sham energy functional, leading to a variational problem for even orders of expansion akin to the zeroth order problem.

3.4.1 Lattice dynamics from electronic-structure theory

The many body Hamiltonian for lattice dynamical properties is given by:

$$(-\Sigma_I \frac{\hbar^2}{2m_I}\frac{\delta^2}{\delta R_j^2} + E(R))\Phi(R) = \epsilon\Phi(R) \tag{3.4.1}$$

where R_I is the coordinate of the Ith nucleus, M_I its mass, R $\equiv R_I$ the set of all the nuclear coordinates, and E(R) the electronic energy of the system, which is often referred to as the Born-Oppenheimer energy surface. It is notice that equilibrium geometry and vibration frequency are first and second derivatives of E(R) respectively. Thus, vanishing interatomic forces of equilibrium forces is:

$$F_I \equiv -\frac{\delta E(R)}{\delta R_I} = 0 \tag{3.4.2}$$

and, lattice vibration frequency ω is the eigenvalues of the Hessian of the Born-Oppenheimer energy, scaled by the nuclear masses:

$$det\left|\frac{1}{\sqrt{M_I M_J}}\frac{\delta^2 E(R)}{\delta R_I R_J} - \omega^2\right| = 0 \tag{3.4.3}$$

However, it is not trival to solve the above Hessian. Hence, we used Hellmann-Fymann theorem as a tool for getting expectation value of the derivatives of eigenvalue.

$$\frac{\delta E_R}{\delta R} = \langle \psi_R \mid \frac{\delta H_R}{\delta R} \mid \psi_R \rangle \tag{3.4.4}$$

where ψ_R is the eigenfunction of H_R corresponding to the E_R eigenvalue: $H_R\psi_R = E_R\psi_R$. The Hessian of the Born-Oppenheimer energy surface appearing in Eq. (3.4.3) is obtained by differentiating the Hellmann-Feynman forces with respect to nuclear coordinates.

From the above argument and Hellmann-Feynman theorem, the first and second derivatives of the ground-state energy reads

$$F_I = \frac{\delta E}{\delta R} = \int \frac{\delta V_R(r)}{\delta R_i} n_R(r) dr \tag{3.4.5}$$

$$\frac{\delta^2 E}{\delta R_i \delta R_j} = \int \frac{\delta^2 V_R(r)}{\delta R_i \delta R_j} n_R(r) dr + \int \frac{\delta n_R(r)}{\delta R_i} \frac{\delta V_R(r)}{\delta R_j} dr \tag{3.4.6}$$

The variation of the Kohn-Sham orbitals, $\Delta\psi_n(r)$, is obtained by standard first-order perturbation theory:

$$(H_{scf} - \epsilon_n) \mid \Delta\psi_n \rangle = -(\Delta V_{scf} - \delta\epsilon_n)|\psi_n\rangle \tag{3.4.7}$$

where

$$n(r) = \Sigma \mid \psi_n(r) \mid^2 \tag{3.4.8}$$

the linearization of the above expression implies that,

$$\Delta n(r) = Re\Sigma\psi_n^*(r)\Delta\psi_n(r) \tag{3.4.9}$$

$$H_{scf} = -\frac{\hbar^2}{2m}\frac{\delta^2}{\delta r^2} + V_{scf}(r) \tag{3.4.10}$$

is the unperturbed kohn-sham Hamiltonian,

$$\Delta V_{scf}(r) = \Delta V(r) + e^2 \int \frac{\Delta n(r')}{\mid r - r' \mid} dr' + \frac{\delta V_{xc}(n)}{\delta n} \mid_{n=n(r)} \Delta n(r) \tag{3.4.11}$$

is the first-order correction to the self-consistent potential, and $\Delta\epsilon_n = \langle\psi_n \mid \Delta V_{scf} \mid \psi_n\rangle$ is the first-order variation of the Kohn-Sham eigenvalue ϵ_n.

From this, the (2n+1) theorem of quantum mechanics allows to calculate the line width ($\Delta\omega$ or γ) by the third order differntial of energy with respect to position. That is the measure of electron-phonon coupling (refers Equation 1.4.2).

3.5 Plane Wave Basis Set

The purpose of a basis set is to allow any arbitrary function ψ to be expressed as a sum of the basis functions ϕ_i.

$$\psi = \sum_i C_i \phi_i \tag{3.5.1}$$

Basically the basis set is said to be complete if this representation of ψ is accurate. If everyone used complete basis sets the only argument would be about the cost of the calculation. But, no one uses a complete basis set. According to the system that computationally analyze,we can choose one of the basis set. So for peridic unit cell implimenting plane wave basis set is better than other basis sets. To apply plane wave basis set it requires pseudopotentials to be efficient which is not all-electron that means core region not included.

Some of the advantage of plane wave basis set are:

- There are very efficient algorithms for performing Fourier transforms allowing calculations to be performed in the most efficient real space or reciprocal space.
- Convergence of physical properties is controlled by a single parameter, the cutoff energy, and can be tested.
- They provide the same accuracy at all points in space.

- The simplicity of plane waves makes it easy to add new functionality to codes and to try alternative algorithms.

3.6 Pseudopotential

When using a plane wave basis set, the region close to an atomic nucleus requires special attention. This is due to two main factors. The first is that the electron-nucleus potential varies as $\frac{1}{r}$ so it diverges as $r \rightarrow 0$. Secondly, to ensure the valence electron wavefunctions are orthogonal to the core electron wavefunctions (as required by the exclusion principle) the valence wavefunctions must oscillate rapidly within the core region. These factors lead to large kinetic energies hence the need for large numbers of plane waves. Also a large number of plane waves are needed to describe the tightly bound core states.

These problems can be circumvented by the use of the pseudopotential approximation. This is motivated by the observation that most physical properties are determined by the valence electrons. The pseudopotential approximation exploits this by removing the core electrons and combining the interaction between the core and valence electrons and the strong nuclear valence electron interaction into a weaker pseudopotential [43]. Within the core region the valence wave functions are then replaced by smoother nodeless pseudo-wavefunctions that are identical to the real wavefunctions outside the core region. This reduces the complexity of the problem in a number of ways. Firstly, removing the core electrons means fewer wavefunctions need to be calculated. Secondly, as the potential no longer diverges

toward $-\infty$ and the valence wave functions are smoother within the core region, fewer plane waves are needed to adequately describe the valence wavefunctions. To ensure that a pseudopotential calculation reproduces the same energy differences as an all-electron calculation it is necessary for the pseudo-wavefunctions to be identical to the all electron wavefunctions outside the core. This condition is called 'norm-conservation'.

Chapter 4

Computational Details

For this thesis work we implimented DFT Quantum espresso computational package and DFPT theory for electron-phonon calculation. In this section we have try to explain the Modeling and simulation procedure for computing superconductivity.

4.1 General Description of QUANTUM ESPRESSO

QUANTUM ESPRESSO implements a variety of methods and algorithms aimed at a chemically realistic modeling of materials from the nanoscale upwards, based on the solution of the density-functional theory (DFT) [35] problem, using a plane waves (PWs) basis set and pseudopotentials (PPs) [44] to represent electron-ion interactions. The codes are constructed around the use of periodic boundary conditions, which allows for a straight forward treatment of infinite crystalline systems, and an efficient convergence to the thermodynamic limit for a periodic but extended system, such as liquids or amorphous materials. Finite systems are also treated using supercells; if required; open-boundary conditions can be used through the use of the density-counter charge method [45]. QUANTUM ESPRESSO can thus be used for any crystal structure or supercell, and for metals

as well as for insulators. The atomic cores can be described by separable [46] norm-conserving (NC) PPs [47], ultrasoft (US) PPs [48], or by projector-augmented wave (PAW) sets [49]. Many different exchange-correlation functionals are available in the framework of the local-density (LDA) or generalized-gradient approximation (GGA) [50], plus advanced functionals like Hubbard U corrections and a few meta-GGA [51] and hybrid functionals [52]. The basic computations/simulations that can be performed include:

• calculation of the Kohn-Sham (KS) orbitals and energies [53] for isolated or extended/periodic systems, and of their ground-state energies;

• complete structural optimizations of the microscopic (atomic coordinates) and macroscopic (unit cell) degrees of freedom, using Hellmann-Feynman forces and stresses [54];

• ground state of magnetic or spin-polarized systems, including spin-orbit coupling [55] and non-collinear magnetism [56];

• ab-initio molecular dynamics (MD), using either the Car-Parrinello Lagrangian [57] or the Hellmann-Feynman forces calculated on the Born-Oppenheimer (BO) surface [34], in a variety of thermodynamical ensembles, including NPT variable -cell [58] MD;

• density functional perturbation theory (DFPT) [41, 42, 59, 60], to calculate second and third derivatives of the total energy at any arbitrary wavelength, providing phonon dispersions, electron-phonon and phonon-phonon interactions, and static response functions (dielectric tensors, Born effective charges, infrared spectra, Raman tensors);

• location of saddle points and transition states via transition-path optimization

using the nudged elastic band (NEB) method [61];

• ballistic conductance within the Landauer-Buttiker theory using the scattering approach [62];

• generation of maximally localized Wannier functions [63] and related quantities;

• calculation of nuclear magnetic resonance (NMR) and electronic paramagnetic resonance (EPR) parameters [64]; and other more advanced calculations are performed.

4.2 Computational Details

In our calculation, we first constructed graphene supercells to investigate the graphene-metal adsorption. The supercells were relaxed. It is again relaxed after adding Sr and Na adatoms. The optimized configurations of the adatom-graphene system are shown in Figure 4.1, 4.2, and 4.3. After the locally stable configurations have been found in the high-symmetry positions, the adatoms are displaced in a direction that fully breaks the symmetry of the system before re-relaxing. The supercells ensure a large distance of about 10 A^0 for the separation between neighbouring adatoms in XY- plane. It is necessary to ensure that the Z-axis of the periodic supercell (perpendicular to the graphene layer) is large enough so that there is no interaction between graphene sheets of adjacent supercell. Then a series of static calculations are performed to determine the interaction potential of adatoms (Sr and Na) with graphene. In this process, the adatoms are kept fixed at different distances depends on the sum of covalent radii along a line perpendicular to the graphene layer. For each adatoms, we optimized the geometry at

each global minimum of total energy curves and then compared the total energy to determine the proper adatom-graphene distance. The relative stabilities of Sr and Na adatom-graphene systems are determined by the adsorption energies.

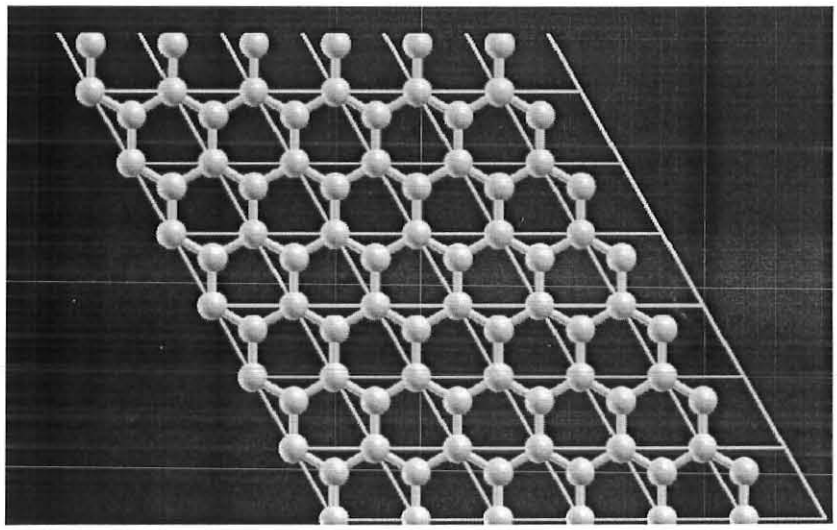

Figure 4.1: Optimized structure of Pristine graphene sheet

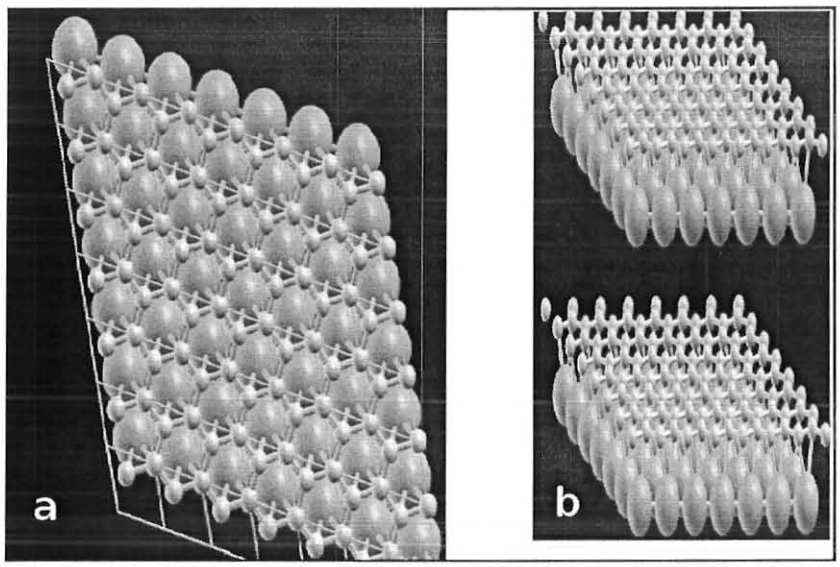

Figure 4.2: Optimized structure of Strontium doped graphene sheet (a)single sheet of Sr-graphene (b) shows the separation distance between Sr-graphene sheets

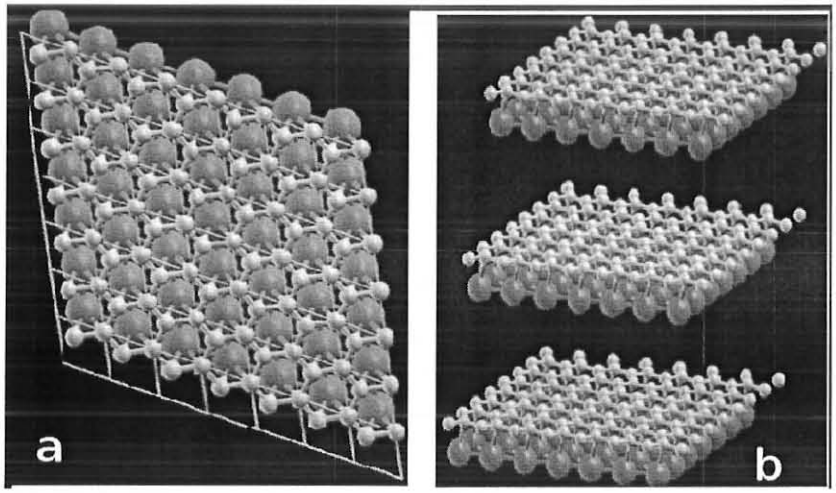

Figure 4.3: Optimized structure of Sodium doped graphene sheet (a)single sheet of Na-graphene (b) shows the separation distance between Na-graphene sheets

All the calculations are performed using density functional theory (DFT) and density functional perturbation theory (DFPT) [18] as implemented in the PWSCF package of the QUANTUM-ESPRESSO distribution [19]. We used the generalised gradient approximation (GGA) [50], norm-conserving pseudo-potentials [21], and a plane-wave expansion up to a 60 Ry cutoff. Brillouin-zone sampling is performed on 8 x 8 x 8 Monkhorst-Pack meshes for graphene, with a Fermi-Dirac smearing in the electronic occupations of 0.02 Ry. We were also calculate the lattice parameter (a) of prestine, Sr-intercalated and Na-intercolated graphen which is 4.255 A^0, 4.275 A^0 and 4.283 A^0, respectively at c = 10 A^0. Then optimization parameters are reported in results and discussions chapter. The monolayer systems were simulated with one adtom (Sr, Na) per unit cell. Phonon frequencies were calculated in DFPT [42, 59, 60] in linear response technique on a phonon wave vector mesh of 8 x 8 x 8 with a 16 x 16 x 16 uniform electron momentum grid. The electron-phonon coupling parameter was calculated with electron mesh momentum K-mesh up to 22 x 22 x 1.

4.3 Computational Procedure in Quantum Espresso

4.3.1 Computational Procedure of Band Structure and Electronic Density of State (EDOS) calculation

The first step is preparing input files for calcualtion. These are:-

[1] gr.scf.in this is an input file for scf calculations.

[2] gr.bands.in this is an input file for collecting bands.

[3] k-point-path this is a file containing list of k-points along symmetry directions in Brillouin zone.

[4] gr.plotband.in this is an input file for putting band structure data into a plottable format.

[5] gr.dos.in this is an input file to calculate density of states.

Then run the input file sequantially, we obtain the corrosponding out put for each input file.

4.3.2 Computational Procedure of Electron-Phonon calculation

This part is illustrates how to calculate electron-phonon interaction coefficients, for a (8 x 8 x 8) Monkhorst-Pack (MP) grid of q-points, in pristin and intercalated graphene.

The calculation proceeds as follows:

[1] Make a self-consistent calculation for all samples using a dense grid of k-points. The dense grid must contain all k and k+q grid points used in the subsequent electron-phonon calculation and must be dense enough to produce accurate electron-phonon coefficients (in particular the double-delta integral at E_F is very

critical). Note that you have to use unshifted grids (k1=k2=k3=0) only, that include k=0! In our case, we uses a (16 16 16) MP grid. (input = name of sample.scf.fit.in, output = name of sample.scf.fit.out)

[2] Make a self-consistent calculation for all samples using a grid of k-points that is suitable for good self-consistency and phonon calculation. For ours case,we uses a (8 8 8) MP grid. (input = name of sample.scf.in, output = name of sample.scf.out)

[3] Make the phonon and electron-phonon calculation for the grid of q-points. Specify elph=.true., and the name of a file where the derivative of the potential is stored "fildvscf". in this case we uses a (8 x 8 x 8) MP grid of q-points (nq1=8, nq2=8, nq3=8). The output contains the results for the el-ph coefficient at each q-point lambda(q), gamma(q), and the double-delta integral at several values of the gaussian broadening. (input = name of sample.elph.in, output = name of sample.elph.out)

[4] Bring to real-space both force constants and el-phon coefficients using "q2r.x" Output in files "a2Fmatdyn.*".

[5] Calculate gamma on selected lines using "matdyn.x" (dos=.false.)

[6] Calculate lambda coefficient (in file "lambda") and the $\alpha^2F(\omega)$ function using "matdyn.x" (dos=.true.)

[7] Calculate lambda coefficient (in "lambda.out") and Tc using "lambda.x"

Chapter 5

RESULTS AND DISCUSSION

Our analysis is started by investigating structural optimization of graphene super cell. Following this, our discussion is extended to the Graphene, Sr-Graphene and Na-Graphene supercell electronic density of states (EDOS), phonon dispersion spectra and phonon density of states (PhDOS). At last, we present the electron-out-of-plane vibration coupling of doped graphene sheet for the response of Eliashberg coupling constant and critical temperature, upon analyzing the electron-phonon coupling Eliashberg fuction in the range less than 900 cm^{-1} which is the only responsible range for phonon mediated superconductivity.

5.1 Structural Optimization

It is rather important for our study to start with structural optimization. From the optimization, we have obtained a stable structure at lowest energy E_T = -22.06 Ry, with Fermi-energy $E_F = -0.64$ Ry at lattice parameter of a = 4.255 A^0 and c = 10 A^0 for pristine graphene sheet. We have measured the bond length of each by using a graphics interface xcrysden. Thus, we have obtained graphene supercell sheet up on error in bond length 10^{-4}.

Table 5.1: Physical parameter of the studied system. Optimized lattice constant(a) and adatom-graphene distance (h) in Å; and Fermi-energy (E_F) and Total energy(E_T) in Rydberge.

Material	a	h	E_F	E_T
Graphene	4.255	–	-0.64	-22.06
Sr-Graphene	4.275	2.68	-0.246	-24.38
Na-Graphene	4.283	2.31	-0.431	-22.81

We have also performed the geometrical optimization and dopant height for doped Sr and Na Graphene sheet with force tolerance value of 0.05 eV/Å which is very small. The optimized results are presented in Table 5.1.

5.1.1 Parameter Optimization

The calculation of many physical quantities such as the total energy of a solid requires integration of functions with Bloch vector k performed over the Brillioun zone (BZ) using the symmetry of the crystal. The integration can be conveniently confined in a smaller region of the BZ, the irreducible wedge of the Brillioun zone (IBZ).

In a plane wave basis set, the single-particle wave functions at each k-point in the BZ of a given crystal that can be expanded in a discrete set of plane waves. In principle, an infinite plane wave basis set is required to expand these wave functions. However, in practical calculations, this set is truncated by an energy cutoff such as only plane waves with kinetic energy $\frac{\hbar^2}{2m}|K+G|^2$ less than energy cutoff are included. Here, the choice of energy cutoff affects the accuracy of the calculations and should be carefully checked with simple convergence tests, i.e. the physical results obtained from the calculations should be converged with respect to this cutoff.

Table 5.2: Optimized parameters: K-point and Energy cutoff (Ry)

Material	K-points	energy cutoff
Graphene	11x11x1	60
Sr-Graphene	8x8x8	60
Na-Graphene	8x8x8	60

In order to decide whether K-point and energy cutoff is more stable, we have carried out the total energy calculations (SCF) for all the structures (Graphene, Sr-Graphene and Na-Graphene). In all cases, we found that the energy is lower for the intercalated structure by preparing a shell/bash scripit in quantum espresso package and we are run it. Thus, we have obatined the following results that are shown in Table 5.2. and the general optimization shown in Figures 5.1 and 5.2.

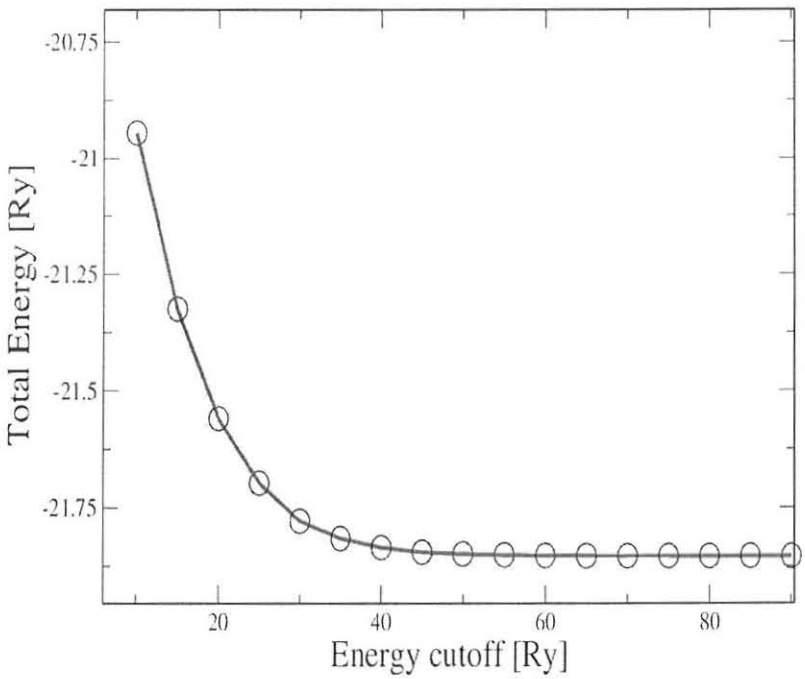

Figure 5.1: Optimization of Energy mesh cuttoff using SCF convergency

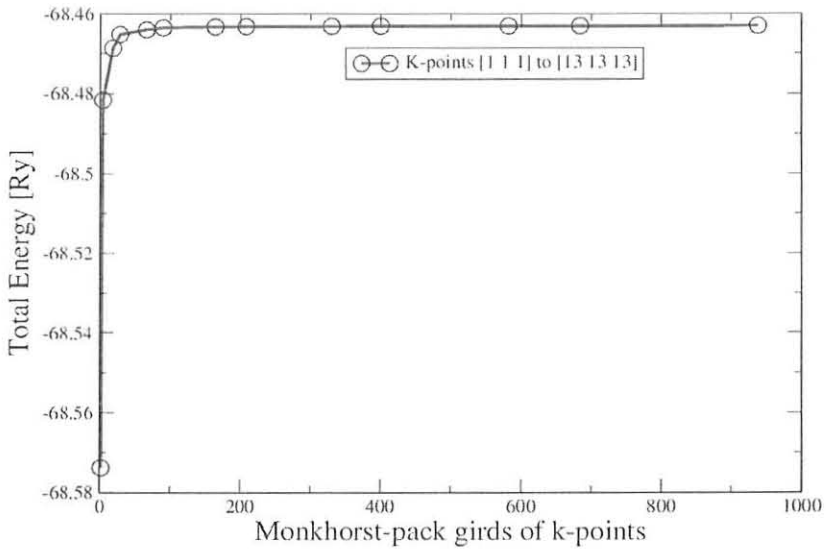

Figure 5.2: Optimized Mesh grid K-points

5.2 Electron Density of State (EDOS)

5.2.1 Electron Density of State (EDOS) of Graphene Sheet

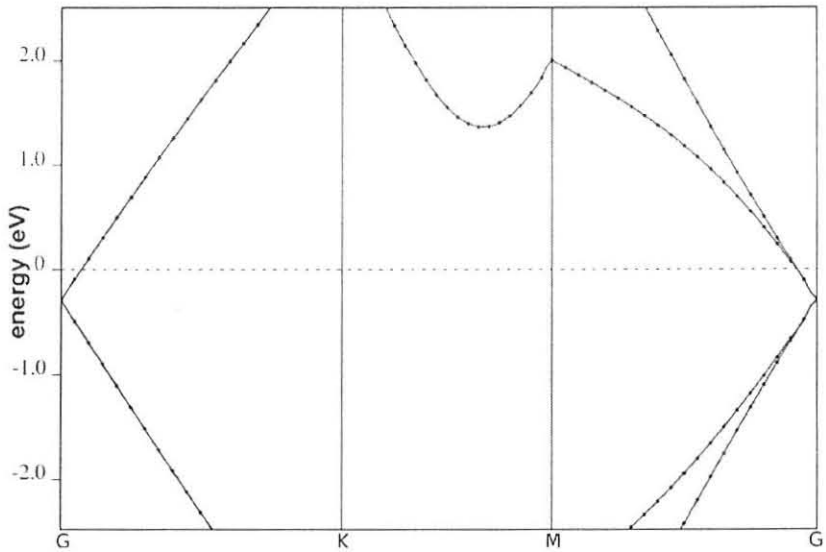

Figure 5.3: Band structure of Pristine graphene Energy in eV *verses* Momentum (where G represent Γ)

According to the band structure of graphene in Figure 5.3, at the Γ-point touch each other, but they do not overlap so that it indicates that pure graphene is a

semi-metallic in nature. In pristine graphene, λ is small and phonon-mediated superconductivity which does not occur as a small number of carriers intrinsic to semi-metallic that leads to vanishingly small N(0) (i.e. N(0) is Electron density of state at fermi-level). In this respect, the situation is similar to the bulk graphite case [65] where without intercalation superconductivity is not stabilized.

In order to establish this fact, we must calculate the Electronic DOS of pristine graphene supercell.

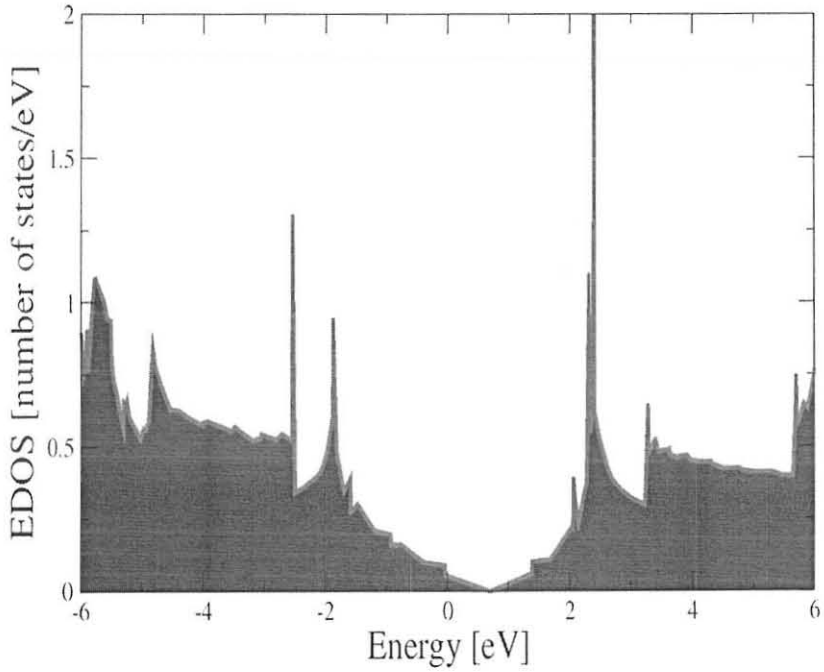

Figure 5.4: Electronic densities of states for pristine graphene

From the EDOS spectra of pristine graphene Figure 5.4, we notice that this material electronic DOS, is very small around the Fermi level (E_F) because it is semi-metallic by nature. Therefore, this material is not expected as a superconductor.

5.2.2 Electron Density of State (EDOS) of Sr-Graphene Sheet

Some research groups have reported that Sr-doped graphite has the ability of having superconductivity [66]. We are thus motivated by this fact that alkaline metals charge transfer to the near materials in a closed vicinity (closed each other) within the covalent radii. Hence, to increase the EDOS and suggest appropriate superconductor in graphene sheet Sr dopant is a good candidate. As of our scope; however, we are the first to study Sr intercalated single sheet of graphene supercell superconductivity. We have presented our EDOS result of Sr-Graphene sheet in Figure 5.5.

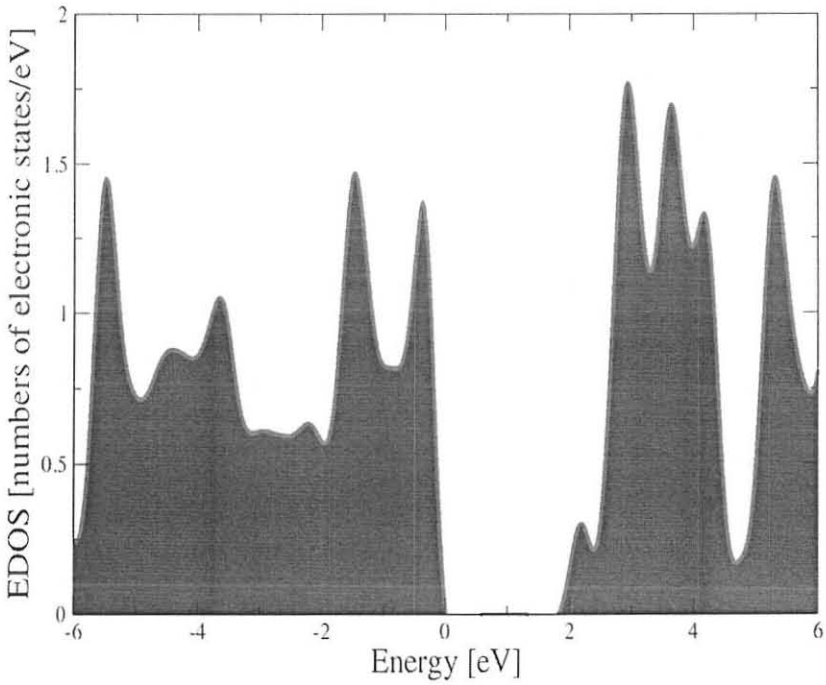

Figure 5.5: Electronic densities of Strontium doped graphene

EDOS of Sr intercalated graphene promotes a new electronic states (DOS is increased) near and at Fermi-level (E_F) as happened in Sr intercalated fullerite [67]

because of the fact that the charge transferred to graphene. Hence, these transferred charges are responsible for conduction and transportation. It has a multiple of beneficial factors on λ [13] the number of carriers enhanced, coupling to carbon out-of-plane vibration is promoted and leads to the material transferred from semi-metallic to a metallic, which is expected from any generic superconductivity. As result, the presence of more interlayer bands (EDOS at fermi is higher) results in strongly softened carbon out of plane vibration [68], which leads to higher coupling of superconductivity.

5.2.3 Electron Density of State (EDOS) of Na-Graphene Sheet

Further, we have performed electron density of state (EDOS) for Na-Graphene sheet, which is shown below in Figure 5.6.

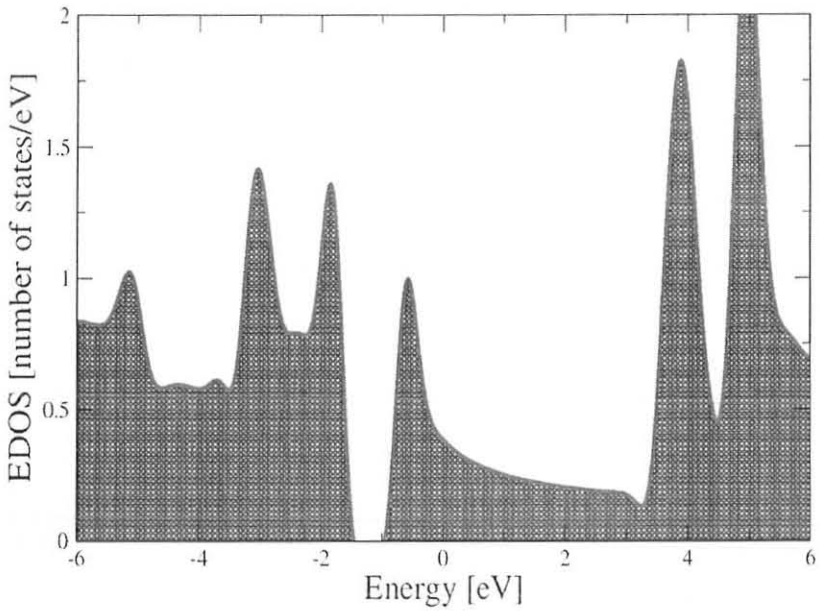

Figure 5.6: Electronic densities of states of Sodium doped graphene

From the EDOS spectrum of Na-Graphene, we can clearly see that the EDOS

at fermi level (E_F) has increased. This indicates that the Na-adsorption leads to charge transfer which is expected to occur between Na and graphene sheet [68]. Hence, the transferred charge has big role in increasing conductivity like that of Sr doped graphene sheet. For this reason, the number of carriers is enhanced coupling to carbon out-of-plane phonon(ZO) is promoted. This is expected from any metallic superconductivity [13].

5.3 Phonon Freqency Dispersion and Phonon Density of States

5.3.1 For the Pristine Graphene Sheet

The Phonon Dispersion energy curve is plotted along the symmetry lines in the hexagonal Brillious zone as shown in Figure 5.7. Basically, in graphene, we can observe 6 modes of vibrations [12]. The corresponding density of states for phonon modes in units of mode perhexagonal unit cell per eV as shown in Figure 5.9. Near to the gamma point (q = 0) (when the momentum is zero), there are three optical branches known as acoustic mode of vibrations. The lowest acoustic branch is an out-of-plane transverse mode (ZA) whose energy varies q^2. There are two inplane acoustic modes with varying energies $|q|$. The lower lying of these two modes is transverse acoustic mode (TA) and the higher lying mode is longitudinal acoustic mode (LA). The lowest lying optical branch an out-of-plane optical mode (ZO) with a negative energy, is dependent on Gamma point. The remaining two branches are inplane transverse (TO) and longitudinal optical (LO) modes which degenerate at the Gamma point. This energy depends on approximately constant

for the small value of q.

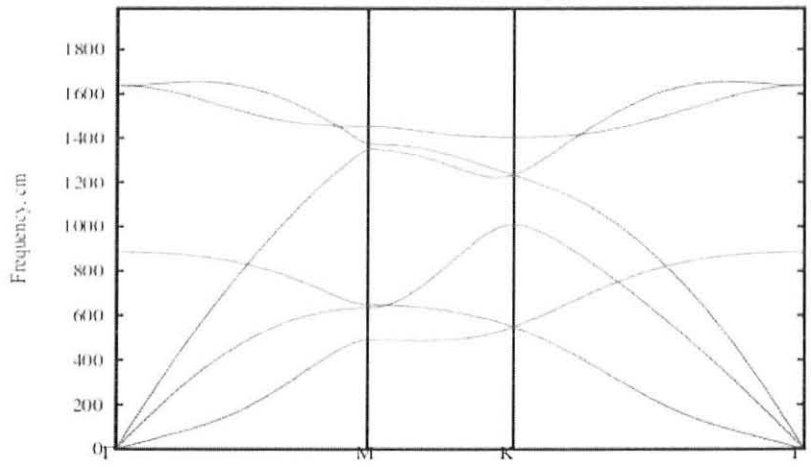

Figure 5.7: Phonon fequency dispersion for pristine graphene

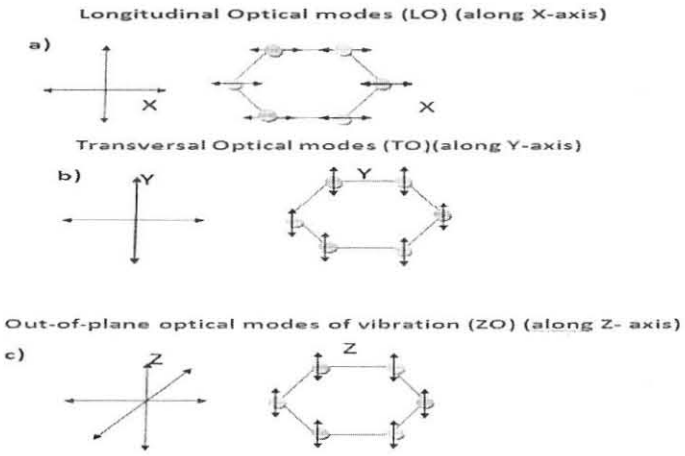

Figure 5.8: Optical phonon modes for Pristine graphene

However, in our case, we mainly focus on Optical modes of vibrations because we are studying superconductivity at symmetry point of the brillouin zone at gamma (Γ). For gamma point LO mode, the carbon atoms of the graphene sheet are placed in XY- plane vibrating in opposite directions parallel to x-axis 180 degree out of phase with each unit cell with each other. For gamma point TO mode, the atom vibrates out of phase parallel to the graphene y-axis. For the gamma point

ZO mode, the sheet vibrates out-of-plane to the graphene XY-placed sheet which is parallel to Z- axis. The mode of displacement vectors for ZO, LO and TO modes are shown schematically in Figure 5.8. In the PhDOS Figure 5.9, we observe that

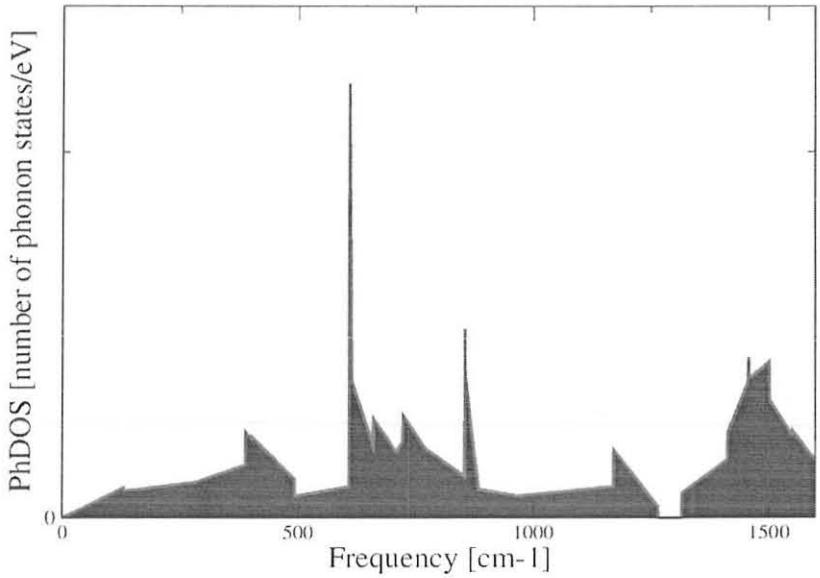

Figure 5.9: Phonon density of states of pristine graphene

there are a few states which are around 650 to 900 cm^{-1}. Hence, phonon state is less in this region for coupling at lower energy which does not takes place even if the in-plane deformation potential of pristine graphene is higher. The reason is that, electron phonon coupling λ is inversely proprtional to omega (frequency) [68]. Because of this fact, one can expect that the critical temperature is also very small which is less than 1K. So that, we cannot expect superconductivity in graphene sheet. In order to estabilish this fact, we have calculated the Eliashberg function $\alpha^2F(\omega)$ at gamma point. This is shown in figure 5.10.

From the Eliashberg functional calculation Figure 5.10, we can observe that there is no electron-phonon coupling takes place in the intermediate energy spectra

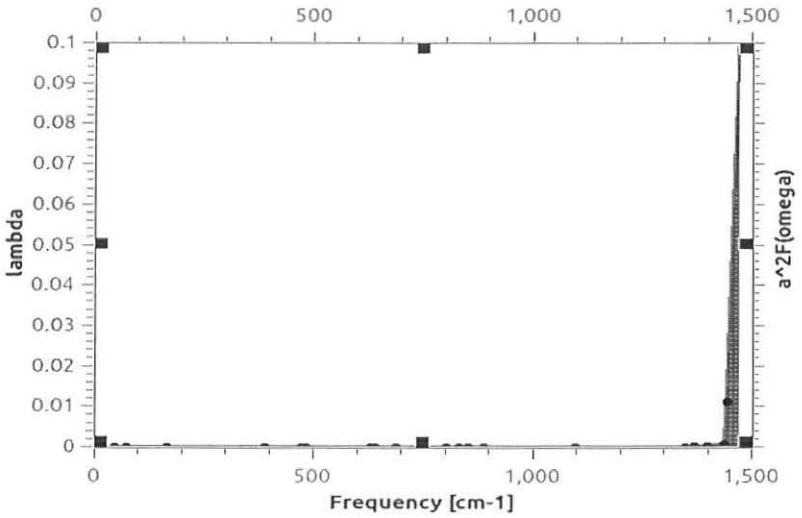

Figure 5.10: Eliashberg function $a^2F(\omega)$ and integral coupling $\lambda(\omega)$

range. This indicates that pristine graphene sheet is not a superconductor which is also supports our EDOS and PhDOS results.

5.3.2 For Sr-Graphene Sheet

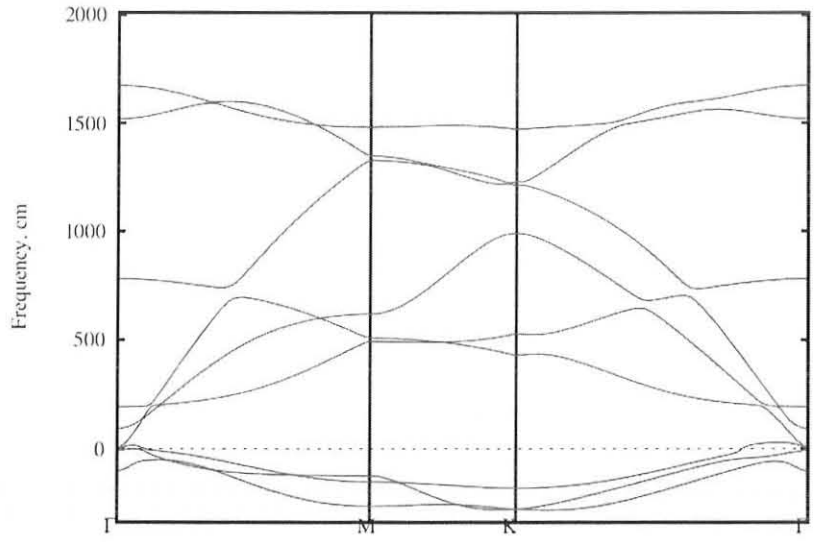

Figure 5.11: Phonon frequency dispersion for Sr-Graphene

From Figure 5.11, we can notice that the Sr intercalation has softened the graphene

out-of-plane phonon (ZO). This leads to more softened ZO which is of highly coupling with the charge transferred from strontium intercalated in the fermi-level. This implies higher critical superconducting temperature T_c. The above result is

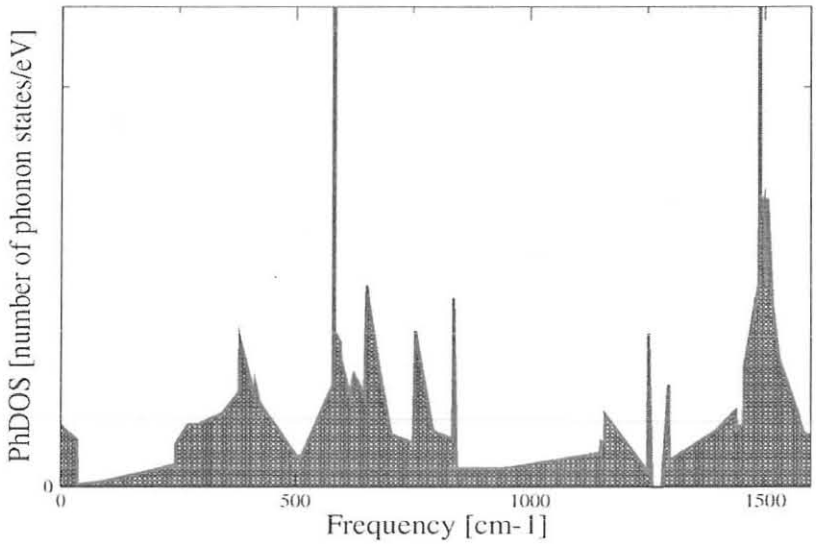

Figure 5.12: Phonon density of states of Sr-graphene

also supported by phonon density of sate plot, which is illustrated in Figure 5.12. From the PhDOS we have observed that the Sr intercalate is softened the out-of-plane phonon vibration (ZO) and seen as a large number of phonon state at around 550 to 600 cm^{-1} in the intermediate energy range which is responsible for electron-phonon coupling in the material. In addition to this, Electronic DOS indicates that the material is transfered from semi-metal to a metal that is expected from any generic superconductivity. So that from the above evidence, we can say that Sr-Graphene sheet is a superconductor.

5.3.3 For Na-Graphene Sheet

Like Sr-Graphene, we have performed the same calculations phonon dispersion and phonon DOS for Na-Graphene material. Hence, we have obtained the following results that are illustarted in the Figure 5.13. From the phonon dispersion

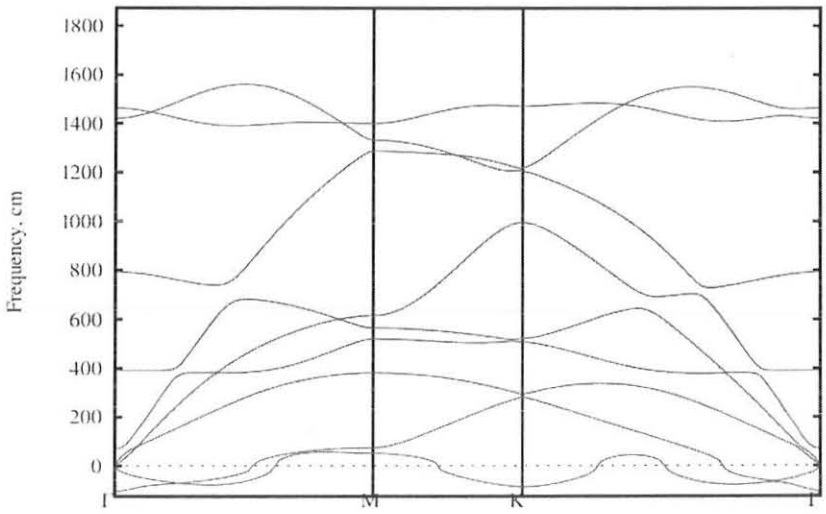

Figure 5.13: Phonon dispersion for Na-graphene

spectra, we notice that the Na intercalate splits the out-of-plane optical phonon in to two vibrations. The more softened ZO is around 400 cm^{-1} and the second rigid ZO mode is found around 800 cm^{-1}. The ZO mode at around 400 cm^{-1} is highly responsible for electron-phonon coupling. These results are also supported by PhDOS of Na-Graphene materials which are schematically represented in Figure 5.14. From the phonon DOS we have noticed that the PhDOS is increased in all the range of the spectra, mostly from 300 to 700 cm^{-1}. This is because of the intercalated sodium atom that softened the out-of-plane optical phonon (ZO). In this material, the more softening of ZO indicates that ZO has higher possibility to couple with the charge that is donated by the intercalated sodium. This implies that this material becomes a good superconductor with higher critical

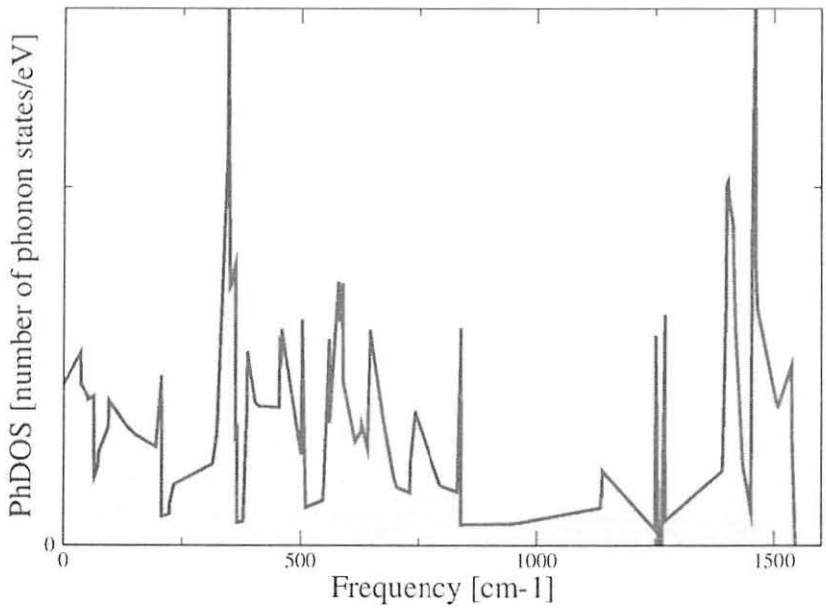

Figure 5.14: Phonon density of states of Na-graphene

temperature.

5.4 Origin of Superconductivity in Doped Graphene Sheet

According to BCS theory, the presence of superconductivity in phonon-mediated superconductors is because of high electron-phonon coupling at lower energy spectra range. In order to induce superconductivity in graphene, doping is necessary to enhance electronic density of states in the fermi-level of the graphene sheet and out-of-plane vibration in the direction to the graphene sheet. Nevertheless, all doping cannot induce superconductivity [68]. Therefore, getting a better intercalant is one of the task in graphene sheet. In the previous section, we have observed that both Sr and Na doped graphene sheet materials are superconductors. To support this fact, we are motivated to calculate electron-phonon

Table 5.3: Optimized lattice constant(a) and adatom-graphene distance (h) in Å; electron-phonon coupling (λ), logarithmic frequency average (ω_{log} in cm^{-1} and superconducting critical temprature (T_C in Keliven) for Sr-graphene and Na-garphene system

Material	a	h	λ	ω_{ln}	T_c
Graphene	4.255	–	0.1	–	< 1
Sr-Graphene	4.275	2.68	0.41	587	2
Na-Graphene	4.283	2.31	0.667	281.25	7.5

coupling and critical temperature by using quantum-espresso software package. The total electron-phonon coupling is the omega that goes to infinity limit of lambda(omega). The results obtained from these calculations are presented in Table 5.3.

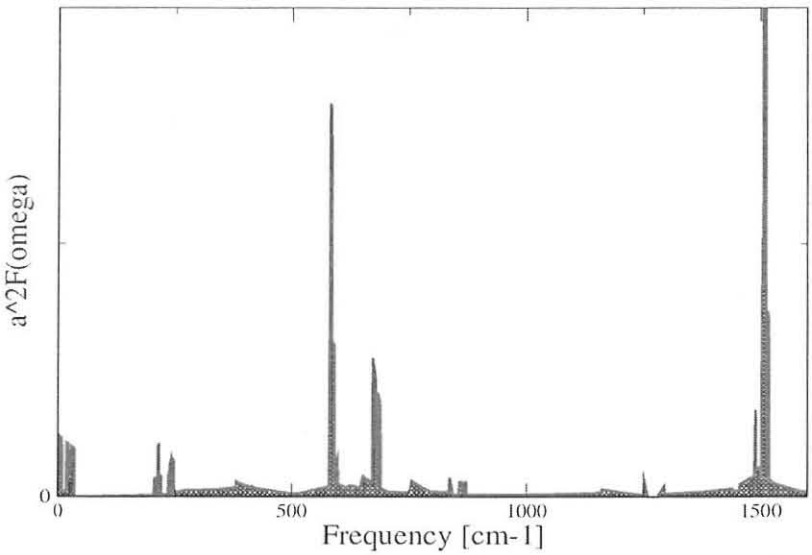

Figure 5.15: Eliashberg functional for Sr-intercalted graphene

Figures 5.12, 5.14, 5.15, and 5.16 are clearly demonstrated why these materials are superconductor. In the calculated phonon density of states (PhDOS) at Figure 5.12 and Eliashberg function $a^2F(\omega)$ Figure 5.15 for strontium intercalated graphene and phonon density of states (PhDOS) at Figure 5.14 and Eliashberg

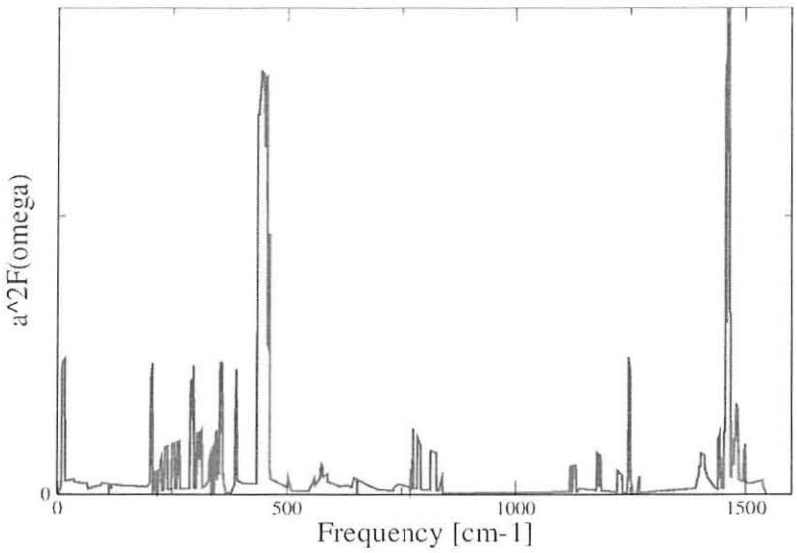

Figure 5.16: Eliashberg function for Na-intercalated graphene

function $a^2F(\omega)$ Figure 5.16 for sodium, we can observe three group of phonons: intercalated related at $\omega \leqslant 200cm^{-1}$, graphene sheet out-of-plane vibration (ZO) around 580 cm^{-1} for Sr-Graphene and 380 cm^{-1} for Na-Graphene, and the in plane vibration of graphene (xy-plane) which is $\geqslant$ 1500 cm^{-1}. The qualitative shape of $a^2F(\omega)$ some how looks similar to the distributions of electron-phonon interaction in the two intercalate. However, the total λ decreases from 0.667 in Na-Graphene to 0.41 in Sr-Graphene sheet, while the logarithmic-average phonon frquency (ω_{ln}) is also changed from 281.25 to 587 cm^{-1} respectively. Other research group has also reported that Sr doped double layer graphene sheet has coupling strength $\lambda = 0.42$ with critical temperature $T_c = 0.95$ K [66]. Comparatively single sheet Sr doped graphene has wide range of superconductivity with similar coupling strength to that of double layer Sr doped graphene.

Using the McMillan-Dynes formula [16], with $\mu^* = 0.115$ taken from litarture [68], we have obtained $T_c = 7.5K$ for Na-Graphene and $T_c = 2$ K for Sr-Graphene.

The reduction of T_c in Sr-Graphene is due to the simultaneous decreasing of transverse vibration of intercalate and the graphene sheet out-of-plane (ZO) is a contribution to the electron-phonon coupling. From this, we can notice that the lower lying inplane vibrations of intercalant has negative impact on T_c but it is also very effective in increasing ω_{ln}. Thus, the effect is partly compensated. On the other hand, the large reduction of coupling associated to out-of-plane optical phonon of graphene sheet happens in higher energy spectra region which has not much contribution to the electron-phonon coupling. This reduces the coupling strength and critical temprature. The reduction of electron-phonon coupling for (ZO) mode of vibration in intermediate region is to explain the significantly lower T_c for Sr-Graphene than Na-Graphene.

Chapter 6

CONCLUSION

In conclusion, we have studied that the occurence of electron-phonon mediated superconductivity in graphene. We have also reported that Na-graphene and Sr-graphene are superconductors at critical temperature of T_c = 7.5 K and 2 K, respectively. In addition to this, we have given a clear evidence that T_c of graphene essentially depends on intercalated to sensitive change of electron-phonon coupling for both in-plane intercalant and out-of-plane graphene phonon(ZO)modes. Last but not least, we have also proved that the strontium and sodium doped graphene are also helpful for inducing superconductivity like that of potassium and calcium intercalated graphene.

REFERENCES

[1] Novoselov, K. S., Andre K. Geim, S. V. Morozov, D. Jiang, Y. Zhang, S. V. Dubonos, I. V. Grigorieva, and A. A. Firsov. "Electric field effect in atomically thin carbon films." Science 306, no. 5696 (2004): 666.

[2] Berger, Claire, Zhimin Song, Xuebin Li, Xiaosong Wu, Nate Brown, Ccile Naud, Didier Mayou et al. "Electronic confinement and coherence in patterned epitaxial graphene." Science 312, no. 5777 (2006): 1191.

[3] Novoselov, K. S., Ak K. Geim, S. V. Morozov, D. Jiang, MI Katsnelson IV Grigorieva, S. V. Dubonos, and A. A. Firsov. "Two-dimensional gas of massless Dirac fermions in graphene." nature 438, no. 7065 (2005): 197.

[4] Heersche, Hubert B., Pablo Jarillo-Herrero, Jeroen B. Oostinga, Lieven MK Vandersypen, and Alberto F. Morpurgo. "Bipolar supercurrent in graphene." Nature 446, no. 7131 (2007): 56.

[5] Ohishi, Megumi, Masashi Shiraishi, Ryo Nouchi, Takayuki Nozaki, Teruya Shinjo, and Yoshishige Suzuki. "Spin injection into a graphene thin film at room temperature." arXiv preprint arXiv:0706.1451 (2007).

[6] Tombros, Nikolaos, Csaba Jozsa, Mihaita Popinciuc, Harry T. Jonkman, and Bart J. Van Wees. "Electronic spin transport and spin precession in single graphene layers at room temperature." Nature 448, no. 7153 (2007): 571.

[7] Ekimov, Evgeny A., Vladimir A. Sidorov, Andrey V. Zoteev, Julia B. Lebed,

Joe D. Thompson, and Sergey M. Stishov. "Structure and superconductivity of isotope-enriched boron-doped diamond." Science and Technology of Advanced Materials 9, no. 4 (2008): 044210.

[8] Csnyi, Gbor, P. B. Littlewood, Andriy H. Nevidomskyy, Chris J. Pickard, and B. D. Simons. "The role of the interlayer state in the electronic structure of superconducting graphite intercalated compounds." Nature Physics 1, no. 1 (2005): 42.

[9] Rosseinsky, M.J., A. P. Ramirez, S. H. Glarum, D. W. Murphy, R. C. Haddon, A. F. Hebard, T. T. M. Palstra, A. R. Kortan, S. M. Zahurak, and A. V. Makhija. "Superconductivity at 28 K in Rbx C60." Physical review letters 66, no. 21 (1991): 2830.

[10] Molitor, Franoise, J. Gttinger, C. Stampfer, S. Drscher, A. Jacobsen, T. Ihn, and K. Ensslin. "Electronic properties of graphene nanostructures." Journal of Physics: Condensed Matter 23, no. 24 (2011): 243201.

[11] Neto, AH Castro, F. Guinea, N. M. R. Peres, K. S. Novoselov, and A. K. Geim. "The electronic properties of graphene." Reviews of modern physics 81, no. 1 (2009): 109.

[12] Saito, Riichiro, Gene Dresselhaus, and Mildred S. Dresselhaus. Physical properties of carbon nanotubes. Vol. 4. London: Imperial college press, 1998.

[13] Profeta, Gianni, Matteo Calandra, and Francesco Mauri. "Phonon-mediated superconductivity in graphene by lithium deposition." Nature Physics (2012):131.

[14] Bardeen, John, Leon N. Cooper, and John Robert Schrieffer. "Theory of superconductivity." Physical Review 108, no. 5 (1957): 1175.

[15] Schrieffer, J. Robert. "John Bardeen and the theory of superconductivity."

Physics Today 45 (1992): 46.

[16] Dressel, Martin, and George Grner. Electrodynamics of solids: optical properties of electrons in matter. Cambridge University Press, 2002.

[17] Emery, Nicolas, Claire Hrold, Jean-Franois March, and Philippe Lagrange. "Synthesis and superconducting properties of CaC6." Science and Technology of Advanced Materials 9, no. 4 (2008): 044102.

[18] Weller, Thomas E., Mark Ellerby, Siddharth S. Saxena, Robert P. Smith, and Neal T. Skipper. "Superconductivity in the intercalated graphite compounds C6Yb and C6Ca." Nature Physics 1, no. 1 (2005): 39.

[19] Calandra, Matteo, and Francesco Mauri. "Theoretical Explanation of Superconductivity in C6Ca." Physical review letters 95, no. 23 (2005): 237002.

[20] Calandra, Matteo, and Francesco Mauri. "Possibility of superconductivity in graphite intercalated with alkaline earths investigated with density functional theory." Physical Review B 74, no. 9 (2006): 094507.

[21] Sanna, A., G. Profeta, A. Floris, A. Marini, E. K. U. Gross, and S. Massidda. "Anisotropic gap of superconducting CaC6: A first-principles density functional calculation." Physical Review B 75, no. 2 (2007): 020511.

[22] Calandra, Matteo, Gianni Profeta, and Francesco Mauri. "Adiabatic and nonadiabatic phonon dispersion in a Wannier function approach." Physical Review B 82, no. 16 (2010): 165111.

[23] Hinks, D. G., D. Rosenmann, H. Claus, M. S. Bailey, and J. D. Jorgensen. "Large Ca isotope effect in the CaC6 superconductor." Physical Review B 75, no. 1 (2007): 014509.

[24] Gonnelli, R. S., Dario Daghero, Debora Delaude, Mauro Tortello, G. A. Ummarino, V. A. Stepanov, J. S. Kim et al. "Evidence for Gap Anisotropy in CaC6 from Directional Point-Contact Spectroscopy." Physical review letters 100, no. 20 (2008): 207004.

[25] Valla, T., J. Camacho, Z-H. Pan, A. V. Fedorov, A. C. Walters, C. A. Howard, and M. Ellerby. "Anisotropic Electron-Phonon Coupling and Dynamical Nesting on the Graphene Sheets in Superconducting CaC6 using Angle-Resolved Photoemission Spectroscopy." Physical review letters 102, no. 10 (2009): 107007.

[26] Meyer, Jannik C., A. K. Geim, M. I. Katsnelson, K. S. Novoselov, T. J. Booth, and S. Roth. "The structure of suspended graphene sheets." Nature 446, no. 7131 (2007): 60.

[27] Jung, Naeyoung, Namdong Kim, Steffen Jockusch, Nicholas J. Turro, Philip Kim, and Louis Brus. "Charge transfer chemical doping of few layer graphenes: charge distribution and band gap formation." Nano letters 9, no. 12 (2009): 4133.

[28] Jung, Naeyoung, Andrew C. Crowther, Namdong Kim, Philip Kim, and Louis Brus. "Raman enhancement on graphene: adsorbed and intercalated molecular species." ACS nano 4, no. 11 (2010): 7005.

[29] Sugawara, K., K. Kanetani, T. Sato, and T. Takahashi. "Fabrication of Li-intercalated bilayer graphene." AIP Advances 1, no. 2 (2011): 022103.

[30] Howard, C. A., M. P. M. Dean, and F. Withers. "Phonons in potassium-doped graphene: The effects of electron-phonon interactions, dimensionality, and adatom ordering." Physical Review B 84, no. 24 (2011): 241404.

[31] Mazin, I. I., and A. V. Balatsky. "Superconductivity in Ca-intercalated bilayer graphene." Philosophical Magazine Letters 90, no. 10 (2010): 731.

[32] Calandra, Matteo, and Francesco Mauri. "Origin of superconductivity of CaC6 and of other intercalated graphites." physica status solidi (b) 243, no. 13 (2006): 3458.

[33] Mourachkine, Andrei. Room-temperature superconductivity. Cambridge Int Science Publishing, 2004.

[34] Kohn, W., Sham, L. J.: Self-consistent equations including exchange and correlation effects. Phys. Rev. 140(4A) (1965):A1133.

[35] Engel, Eberhard, and Reiner M. Dreizler. Density Functional Theory: An Advanced Course. Springerverlag Berlin Heidelberg, 2011.

[36] Hohenberg, Pierre, and Walter Kohn. "Inhomogeneous electron gas." Physical Review 136, no. 3B (1964): B864.

[37] Sholl, David, and Janice A. Steckel. Density functional theory: a practical introduction. Wiley-Interscience, 2011.

[38] von Barth, Ulf, and Lars Hedin. "A local exchange-correlation potential for the spin polarized case. i." Journal of Physics C: Solid State Physics 5, no. 13 (1972): 1629.

[39] Gunnarsson, Olle, and B. I. Lundqvist. "Exchange and correlation in atoms, molecules, and solids by the spin-density-functional formalism." Physical Review B 13, no. 10 (1976): 4274.

[40] Patteson, James D., James Deane Patterson, and Bernard C. Bailey. Solid-state physics: introduction to the theory. Springer Verlag, 2007. [41] Baroni, Stefano, Paolo Giannozzi, and Andrea Testa. "Greens-function approach to linear response in solids." Physical review letters 58, no. 18 (1987): 1861.

[42] Gonze, Xavier. "Adiabatic density-functional perturbation theory." Physical

Review A 52, no. 2 (1995): 1096.

[43] Yin, M. T., and Marvin L. Cohen. "Theory of ab initio pseudopotential calculations." Physical Review B 25, no. 12 (1982): 7403.

[44] Pickett, Warren E. "Pseudopotential methods in condensed matter applications." Computer Physics Reports 9, no. 3 (1989): 115.

[45] Dabo, Ismaila, Boris Kozinsky, Nicholas E. Singh-Miller, and Nicola Marzari. "Electrostatics in periodic boundary conditions and real-space corrections." Physical Review B 77, no. 11 (2008): 115139.

[46] Kleinman, Leonard, and D. M. Bylander. "Efficacious form for model pseudopotentials." Physical Review Letters 48, no. 20 (1982): 1425.

[47] Hamann, D. R., M. Schlter, and C. Chiang. "Norm-conserving pseudopotentials." Physical Review Letters 43, no. 20 (1979): 1494.

[48] Vanderbilt, David. "Soft self-consistent pseudopotentials in a generalized eigenvalue formalism." Physical Review B 41, no. 11 (1990): 7892.

[49] Blchl, Peter E. "Projector augmented-wave method." Physical Review B 50, no. 24 (1994): 17953.

[50] Perdew, John P., J. A. Chevary, S. H. Vosko, Koblar A. Jackson, Mark R. Pederson, D. J. Singh, and Carlos Fiolhais. "Atoms, molecules, solids, and surfaces: Applications of the generalized gradient approximation for exchange and correlation." Physical Review B 46, no. 11 (1992): 6671.

[51] Tao, Jianmin, John P. Perdew, Viktor N. Staroverov, and Gustavo E. Scuseria. "Climbing the density functional ladder: Nonempirical metageneralized gradient approximation designed for molecules and solids." Physical Review Letters 91, no. 14 (2003): 146401.

[52] Dickson, Ross M., and Axel D. Becke. "Basissetfree local densityfunctional calculations of geometries of polyatomic molecules." The Journal of chemical physics 99 (1993): 3898.

[53] Kohn, Walter, and Lu Jeu Sham. Self-consistent equations including exchange and correlation effects. Defense Technical Information Center, 1965. [54] Feynman, R. P. "Forces in molecules." Physical Review 56, no. 4 (1939): 340

[55] Pyykko, Pekka. "Relativistic effects in structural chemistry." Chemical Reviews 88, no. 3 (1988): 563.

[56] Gebauer, Ralph, and Stefano Baroni. "Magnons in real materials from density-functional theory." Physical Review B 61, no. 10 (2000): R6459.

[57] Car, Richard, and Mark Parrinello. "Unified approach for molecular dynamics and density-functional theory." Physical review letters 55, no. 22 (1985): 2471.

[58] Fischer, D. A., R. M. Wentzcovitch, R. G. Carr, A. Continenza, and A. J. Freeman. "Graphitic interlayer states: A carbon K near-edge x-ray-absorption fine-structure study." Physical Review B 44, no. 3 (1991): 1427.

[59] Baroni, Stefano, Paolo Giannozzi, and Andrea Testa. "Elastic constants of crystals from linear-response theory." Physical review letters 59, no. 23 (1987): 2662.

[60] Baroni, Stefano, Stefano de Gironcoli, Andrea Dal Corso, and Paolo Giannozzi. "Phonons and related crystal properties from density-functional perturbation theory." Reviews of Modern Physics 73, no. 2 (2001): 515.

[61] Weinan, E., Weiqing Ren, and Eric Vanden-Eijnden. "String method for the study of rare events." Physical Review B 66, no. 5 (2002): 052301.

[62] Delaney, Paul, Hyoung Joon Choi, Jisoon Ihm, Steven G. Louie, and Marvin

L. Cohen. "Broken symmetry and pseudogaps in ropes of carbon nanotubes." Physical Review B 60, no. 11 (1999): 7899.

[63] Souza, Ivo, Nicola Marzari, and David Vanderbilt. "Maximally localized Wannier functions for entangled energy bands." Physical Review B 65, no. 3 (2001): 035109.

[64] Pickard, Chris J., and Francesco Mauri. "Nonlocal pseudopotentials and magnetic fields." Physical review letters 91, no. 19 (2003): 196401.

[65] Ooi, Newton, Asit Rairkar, and James B. Adams. "Density functional study of graphite bulk and surface properties." Carbon 44, no. 2 (2006): 231.

[66] Jishi, R. A., D. M. Guzman, and H. M. Alyahyaei. "Theoretical investigation of two-dimensional superconductivity in intercalated graphene layers." arXiv preprint arXiv:1107.1845 (2011).

[67] Kortan, A. R., N. Kopylov, E. zdas, A. P. Ramirez, R. M. Fleming, and R. C. Haddon. "Strontium doped fullerite compounds." Chemical physics letters 223, no. 5 (1994): 501.

[68] Calandra, Matteo, Gianni Profeta, and Francesco Mauri. "Superconductivity in metalcoated graphene." physica status solidi (b) 249, no. 12 (2012): 2544.

[69] Valla, Tonica, and Zhihui Pan. "Superconductivity and Electron-Phonon Coupling in Graphite Intercalation Compunds." Physics and Applications of Graphene-Experiments (in-Tech, 2011):455.